UNIVERSITY OF BIRMINGHAM
University of Birmingham Research at Birmingham

Nucleic acid–protein interfaces studied by MAS solid-state NMR spectroscopy

Aguion, Philipp Innig; Marchanka, Alexander; Carlomagno, Teresa

DOI:
10.1016/j.yjsbx.2022.100072

License:
Creative Commons: Attribution-NonCommercial-NoDerivs (CC BY-NC-ND)

Document Version
Publisher's PDF, also known as Version of record

Citation for published version (Harvard):
Aguion, PI, Marchanka, A & Carlomagno, T 2022, 'Nucleic acid–protein interfaces studied by MAS solid-state NMR spectroscopy', *Journal of Structural Biology: X*, vol. 6, 100072. https://doi.org/10.1016/j.yjsbx.2022.100072

Link to publication on Research at Birmingham portal

General rights
Unless a licence is specified above, all rights (including copyright and moral rights) in this document are retained by the authors and/or the copyright holders. The express permission of the copyright holder must be obtained for any use of this material other than for purposes permitted by law.

•Users may freely distribute the URL that is used to identify this publication.
•Users may download and/or print one copy of the publication from the University of Birmingham research portal for the purpose of private study or non-commercial research.
•User may use extracts from the document in line with the concept of 'fair dealing' under the Copyright, Designs and Patents Act 1988 (?)
•Users may not further distribute the material nor use it for the purposes of commercial gain.

Where a licence is displayed above, please note the terms and conditions of the licence govern your use of this document.

When citing, please reference the published version.

Take down policy
While the University of Birmingham exercises care and attention in making items available there are rare occasions when an item has been uploaded in error or has been deemed to be commercially or otherwise sensitive.

If you believe that this is the case for this document, please contact UBIRA@lists.bham.ac.uk providing details and we will remove access to the work immediately and investigate.

Download date: 23. Apr. 2024

Journal of Structural Biology: X 6 (2022) 100072

Contents lists available at ScienceDirect

Journal of Structural Biology: X

journal homepage: www.sciencedirect.com/journal/journal-of-structural-biology-x

Research Article

Nucleic acid–protein interfaces studied by MAS solid-state NMR spectroscopy

Philipp Innig Aguion [a], Alexander Marchanka [a,b], Teresa Carlomagno [c,*]

[a] Institute for Organic Chemistry and Centre of Biomolecular Drug Research (BMWZ), Leibniz University Hannover, Schneiderberg 38, 30167 Hannover, Germany
[b] Structural and Computational Biology Unit, European Molecular Biology Laboratory, Meyerhofstr. 1, 69117 Heidelberg, Germany
[c] School of Biosciences/College of Life and Enviromental Sciences, Institute of Cancer and Genomic Sciences/College of Medical and Dental Sciences, University of Birmingham, Edgbaston, Birmingham B15 2TT, UK

ARTICLE INFO

Keywords:
ssNMR
Nucleic acid-protein complexes
Intermolecular interfaces

ABSTRACT

Solid-state NMR (ssNMR) has become a well-established technique to study large and insoluble protein assemblies. However, its application to nucleic acid–protein complexes has remained scarce, mainly due to the challenges presented by overlapping nucleic acid signals. In the past decade, several efforts have led to the first structure determination of an RNA molecule by ssNMR. With the establishment of these tools, it has become possible to address the problem of structure determination of nucleic acid–protein complexes by ssNMR. Here we review first and more recent ssNMR methodologies that study nucleic acid–protein interfaces by means of chemical shift and peak intensity perturbations, direct distance measurements and paramagnetic effects. At the end, we review the first structure of an RNA–protein complex that has been determined from ssNMR-derived intermolecular restraints.

Introduction

Besides its long-established role as carrier of genetic information in protein translation, RNA acts in many other cellular contexts, with new roles being discovered regularly (Cech and Steitz, 2014). The vast majority of the RNAs made from the human genome have distinct functions from protein coding (non-coding RNAs, ncRNAs), but many of these functions remain unknown. Both coding RNA (mRNA) and ncRNAs may act in complex with specific RNA-binding proteins (RPBs), which contain well-defined RNA recognition motifs (Corley et al., 2020). Being involved in such high number of biological functions, RNA molecules hold potentials as both therapeutic agents and targets.

As for proteins, the development of RNAs either as therapeutic targets or as protein-targeting agents requires understanding their three-dimensional structures and their interaction modes with proteins. Methods to characterize RNA–protein interactions develop rapidly (Schlundt et al., 2017). X-ray crystallography and cryo electron microscopy (cryo-EM) can be applied to high molecular-weight complexes and have been the methods of choice to study many large ribonucleoprotein complexes (RNPs) in the past years (Ben-Shem et al., 2011; Ghanim et al., 2021; Jackson et al., 2014; Khatter et al., 2015; Nguyen et al., 2016). These techniques work well for RNPs with well-defined structures but fall short when addressing conformational heterogeneity or dynamic processes. RNA molecules can adopt different folds depending on both the environmental conditions and the interacting partners and are often flexible in isolation. The presence of disordered RNA regions can make crystallization of RNPs quite challenging (Blanco and Montoya, 2011), while cryo-EM analysis remains blind to disordered molecular regions. In addition, both X-ray crystallography and cryo-EM are unable to represent the dynamics of the studied system at atomic level, which, especially in enzymes, provides the crucial link between structure and function. Finally, several intermolecular interactions with functional regulatory roles are transient in nature; transient complexes are difficult to crystallize and may dissociate during the preparation of cryo-EM grids, rendering both X-ray crystallography and cryo-EM inapplicable.

NMR spectroscopy is a structural biology technique that is able to provide structural information in the presence of disorder and dynamics. As such, NMR is very useful to study RNPs, and more generally nucleic acid–protein complexes, containing flexible regions, and reveals whether and how these disordered regions contribute to binding specificity and/or modulate affinity. NMR spectroscopy also enables structural studies of transiently forming complexes in a wide range of affinities (Campagne et al., 2011; Carlomagno, 2014; Dominguez et al.,

* Corresponding author.
E-mail address: t.carlomagno@bham.ac.uk (T. Carlomagno).

https://doi.org/10.1016/j.yjsbx.2022.100072
Received 16 June 2022; Received in revised form 11 August 2022; Accepted 15 August 2022
Available online 18 August 2022
2590-1524/© 2022 The Authors. Published by Elsevier Inc. This is an open access article under the CC BY-NC-ND license (http://creativecommons.org/licenses/by-nc-nd/4.0/).

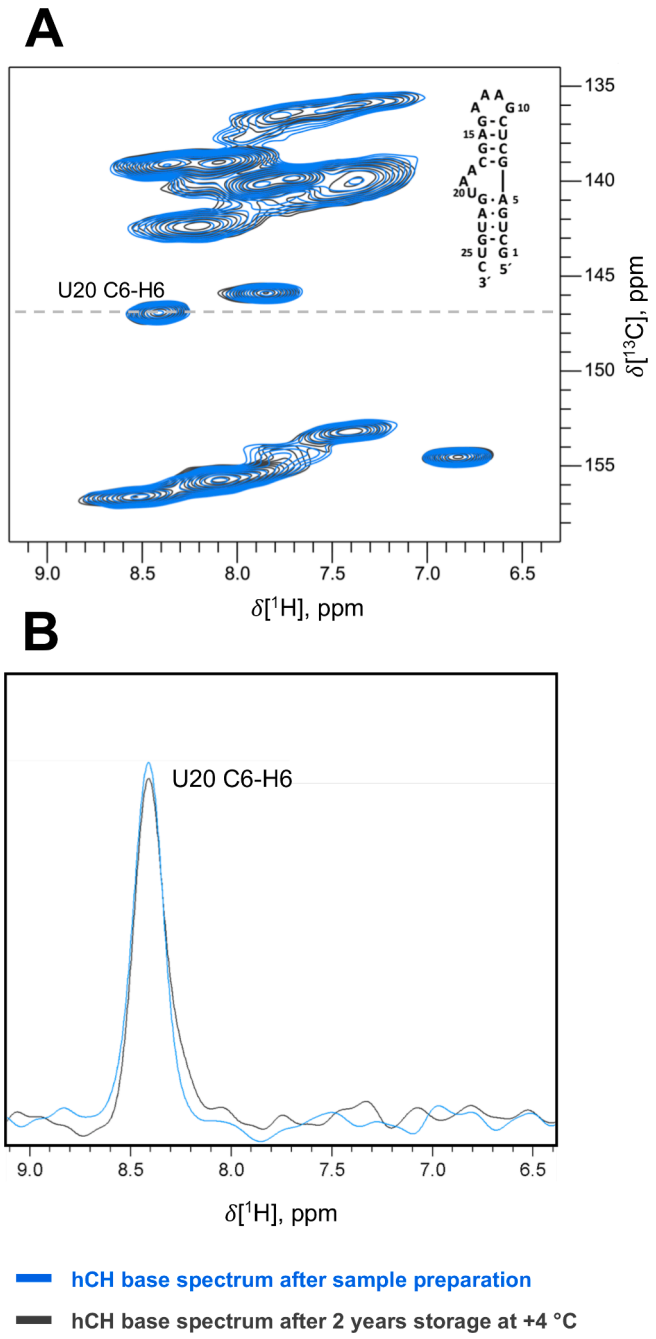

Fig. 1. Long-term stability of precipitated RNP samples. **(A)** Overlay of the 2D CP hCH spectra tailored for the base spectral region of uniformly ^{13}C,^{15}N labeled *Pyrococcus furiosus (Pf)* 26mer Box C/D RNA in complex with the *Pf* L7Ae protein (Aguion et al., 2021; Marchanka et al., 2018b) immediately after sample preparation (blue) and two years after storage at + 4 °C (grey). **(B)** Representative horizontal 1D trace of the C6-H6 peak from residue U20 taken from the 2D spectra at the indicated dashed line in **(A)**. Peaks after two years of storage at + 4 °C show only minimal loss of signal intensity. Spectra were recorded on a Bruker Avance III HD spectrometer at a ^{1}H resonance frequency of 850 MHz, a magic angle spinning (MAS) rate of 100 kHz, and a temperature of 275 K, using a 0.81-mm MAS probe-head developed by the Samoson group (https://www.nmri.eu/). The measurement time for both experiments was 7.5 h and all acquisition and processing parameters were the same as described in detail in (Aguion et al., 2021).

Table 1
Nuclei relevant for the identification of nucleic acid–protein binding interfaces in ssNMR.

Nuclei	Spin quantum number	Natural abundance (%)	Gyromagnetic ratio γ (10^7 rad T^{-1} s^{-1})	NMR transition frequency at 18.8 T (MHz)
^{1}H	½	99.98	26.7519	800
^{2}H	1	0.015	4.1066	123
^{13}C	½	1.1	6.7283	200
^{15}N	½	0.37	−2.7126	80
^{19}F	½	100	25.1815	753
^{31}P	½	100	10.8394	324

2011; Simon et al., 2011; Yadav and Lukavsky, 2016). Finally, NMR allows the direct observation of hydrogen atoms, which remain inaccessible by X-ray crystallography or cryo-EM but play a crucial role in nucleic acids interactions (Yip et al., 2020).

Notoriously, NMR studies in solution are limited to particles of less than ~ 50 kDa, due to the direct dependency of line-broadening on the molecular size. For proteins, this limit has been considerably extended by the methyl-TROSY methodology (transverse relaxation-optimized spectroscopy) (Kay, 2011; Rosenzweig and Kay, 2014; Tugarinov et al., 2003) in combination with selective $^{13}CH_3$ methyl group labeling of highly deuterated proteins. Methyl-TROSY NMR exploits the excellent relaxation properties of methyl groups, which, when present as only hydrogen-bearing groups in otherwise deuterated proteins, retain feasible NMR line widths even in particles as large as 1 MDa (Lapinaite et al., 2013; Mas et al., 2018, 2013; Sprangers and Kay, 2007; Graziadei et al., 2020). Unfortunately, RNAs do not contain any methyl groups and NMR studies of large RNAs rely on a challenging combination of two-dimensional ^{1}H–^{1}H correlation experiments measured on several selectively-deuterated samples (Brown et al., 2020; Keane et al., 2015). Recently, methyl-TROSY has been applied to high-molecular weight DNA, where methyl groups were engineered at the C5 and N6 positions of cytosines (5mC) and adenines (6 mA) (Abramov et al., 2020). However, because artificial methylation of both DNA and RNA can affect their structures, dynamics and interactions with binding partners (Choy et al., 2010; Helm, 2006; Kawai et al., 1992; Ngo et al., 2016; Williams et al., 2001), nucleic acids methylation cannot be generally applicable to study large nucleic acids by NMR. In fact, methylation of both DNA and RNA occurs naturally in the cell, where it exerts a regulatory function by modulating both the structure and the interactome of nucleic acids.

Solid-state NMR spectroscopy (ssNMR) is another form of biomolecular NMR spectroscopy, which has been applied extensively to insoluble and non-crystalline particles, such as membrane proteins (Cady et al., 2010; Lange et al., 2006; Park et al., 2012; Shahid et al., 2012; Shi et al., 2009) and amyloid fibrils (Colvin et al., 2016; Hoop et al., 2016; Tycko, 2011; Van Melckebeke et al., 2010). ssNMR linewidths do not depend on the molecular weight, making the application of ssNMR to large particles feasible, provided that there is enough signal to compensate for the small number of large particles that can be fitted into a rotor of a given size. In addition, because ssNMR lines are intrinsically broader than solution NMR lines, selective isotope labeling is often crucial to resolve spectral overlaps and achieve site-specific assignment also of moderately sized molecules. Despite these limitations, ssNMR has been applied to large viral assemblies (Andreas et al., 2016; Goldbourt et al., 2007; Lusky et al., 2021; Morag et al., 2015, 2014; Sergeyev et al., 2011; Yu and Schaefer, 2008) and site specific structural information was obtained for the 46-residue-long major coat protein subunit of the filamentous bacteriophage Pf1, as part of the 36 MDa virion (Goldbourt et al., 2007), thanks to the fact that the 7300 subunits of the virion all adopt the same conformation. Over the years, the ssNMR toolbox has been extended for the application to RNA in isolation (Leppert et al., 2004; Lusky et al., 2021; Riedel et al., 2006, 2005a,2005b; Yang et al., 2017), RNA bound to short peptides (Huang et al., 2010, 2011, 2017,

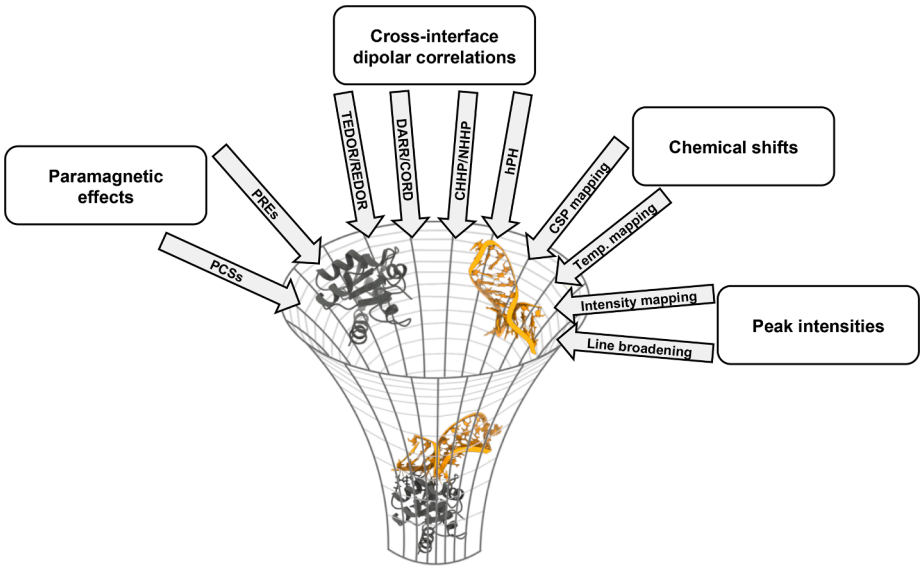

Fig. 2. Overview of ssNMR methods utilized to date to probe nucleic acid–protein interfaces. Information derived from paramagnetic effects, cross-interface dipolar correlations, chemical shifts and peak intensities are highly complementary and can be utilized as restraints in a molecular docking protocol that builds the nucleic acid–protein complex from the structures of the individual components. Pseudo contact shifts (PCSs) measure changes in chemical shifts due to the influence of a paramagnetic ion with anisotropic tensor. Paramagnetic relaxation enhancement (PRE) measures the increase in relaxation of nuclei in the vicinity of an unpaired electron. Both effects can be quantified and translated into nucleus-electron distances. Cross-interface dipolar correlations directly measure intermolecular distances through a variety of dipolar recoupling techniques. The ssNMR toolbox for the measurement of intermolecular distances covers transferred echo double resonance (TEDOR)/ rotational echo double resonance (REDOR)-based recoupling experiments, ^{13}C–^{13}C correlation experiments, such as dipolar assisted rotational resonance (DARR) and combined $R2_n^v$-driven (CORD), spin-diffusion based CHHP/NHHP experiments, and ^{1}H-detected CP-based hPH experiments. Chemical shift perturbation (CSP) mapping reports on changes in chemical shifts occurring in the protein upon binding of the nucleic acid, while temperature mapping measures the temperature dependence of ^{1}H chemical shifts, which in turn depends on the involvement of the atom in hydrogen bonds. Comparison of temperature coefficients in the free and nucleic acid-bound states can reveal which protein residues are involved in nucleic acid binding. Quantification of peak intensities can also reveal which atoms are close to the partner molecule in the complex, because of binding-induced line-broadening effects.

Table 2
Selection of ssNMR studies of intermolecular interactions in nucleic acid–protein complexes since 2005.

Year	Reference	Complex type	Site specific information	Protein (aa)	NA (nt)	ssNMR technique
2005	(Olsen et al., 2005)	1:1 dsRNA–peptide	Yes	11	29	^{31}P-^{19}F REDOR
2008	(Yu and Schaefer, 2008)	dsDNA–protein (intact bacteriophage)	No	not known	342,000	^{15}N-^{31}P, ^{31}P-^{15}N REDOR
2010	(Jehle et al., 2010)	1:1 dsRNA–protein	Yes	123	26	^{31}P-^{15}N TEDOR
	(Huang et al., 2010)	1:1 dsRNA–peptide	Yes	11	29	^{13}C/^{15}N-^{19}F REDOR
2011	(Huang et al., 2011)	1:1 dsRNA–peptide	Yes	11	29	^{13}C-^{31}P, ^{13}C-^{19}F, ^{15}N-^{31}P, ^{15}N-^{19}F, ^{31}P-^{19}F REDOR
	(Sergeyev et al., 2011)	ssDNA–protein (intact bacteriophage)	Partially (only for coat protein)	46	7349	^{13}C,^{13}C DARR
	(Bechinger et al., 2011)	Oligomeric dsDNA–peptide	No	27	not known	^{15}N-^{31}P REDOR
2013	(Asami et al., 2013)	1:1 dsRNA–protein	Yes	123	26	Intensity mapping (Dipolar-coupling-mediated line broadening)
2014	(Morag et al., 2014)	ssDNA–protein (intact bacteriophage)	Partially (only for coat protein)	50	8233	^{13}C,^{13}C CORD/DARR, PHHC
2016	(Wiegand et al., 2016)	2:12:12 ssDNA–protein–AMP-PNP	Yes	521	20	CSP (1D ^{1}H ^{31}P CP, ^{13}C,^{13}C DARR)
2017	(Wiegand et al., 2017b)	2:12:12 ssDNA–protein–ADP	No	521	20	2D PC-C, 2D PHHC-C
2019	(Wiegand et al., 2019)	2:12:12 ssDNA–protein–AMP-PCP/ ADP:AlF_4/ATP/ADP	Yes	521	20	CSP (1D ^{1}H ^{31}P CP, ^{13}C,^{13}C DARR, 2D CP ^{13}C-^{15}N), Intensity mapping (^{13}C,^{13}C DARR), NHHP
	(Boudet et al., 2019)	1:1:2 ssDNA–-protein–ATP	Yes	331	9	CSP (^{13}C,^{13}C DARR, 2D CP ^{13}C-^{15}N), CHHP, NHHP
2020	(Wiegand et al., 2020b)	2:12:12 ssDNA–protein– ADP:AlF_4/ AMP-PCP	Yes	521	20	NHHP, CHHP, CSP (CP-hNH), Intensity mapping (^{31}P,^{31}P DARR)
	(Lacabanne et al., 2020)	1:1:2 ssDNA–protein–ATP	Yes	331	9	CSP (CP-hNH, CP-hCH), Intensity mapping (CP-hNH)
	(Ahmed et al., 2020)	Monomeric dsRNA–protein	Yes	123	26	PRE, CSP (^{13}C,^{13}C DARR, 2D CP ^{13}C-^{15}N)
2021	(Zehnder et al., 2021)	2:12:12 ssDNA–protein–ADP:AlF_4	Yes	521	20	PRE
	(Malär et al., 2021b)	2:12:12 ssDNA–protein–ADP:AlF_4	Yes	521	20	CP-hPH, CSP temperature mapping (CP-hNH)

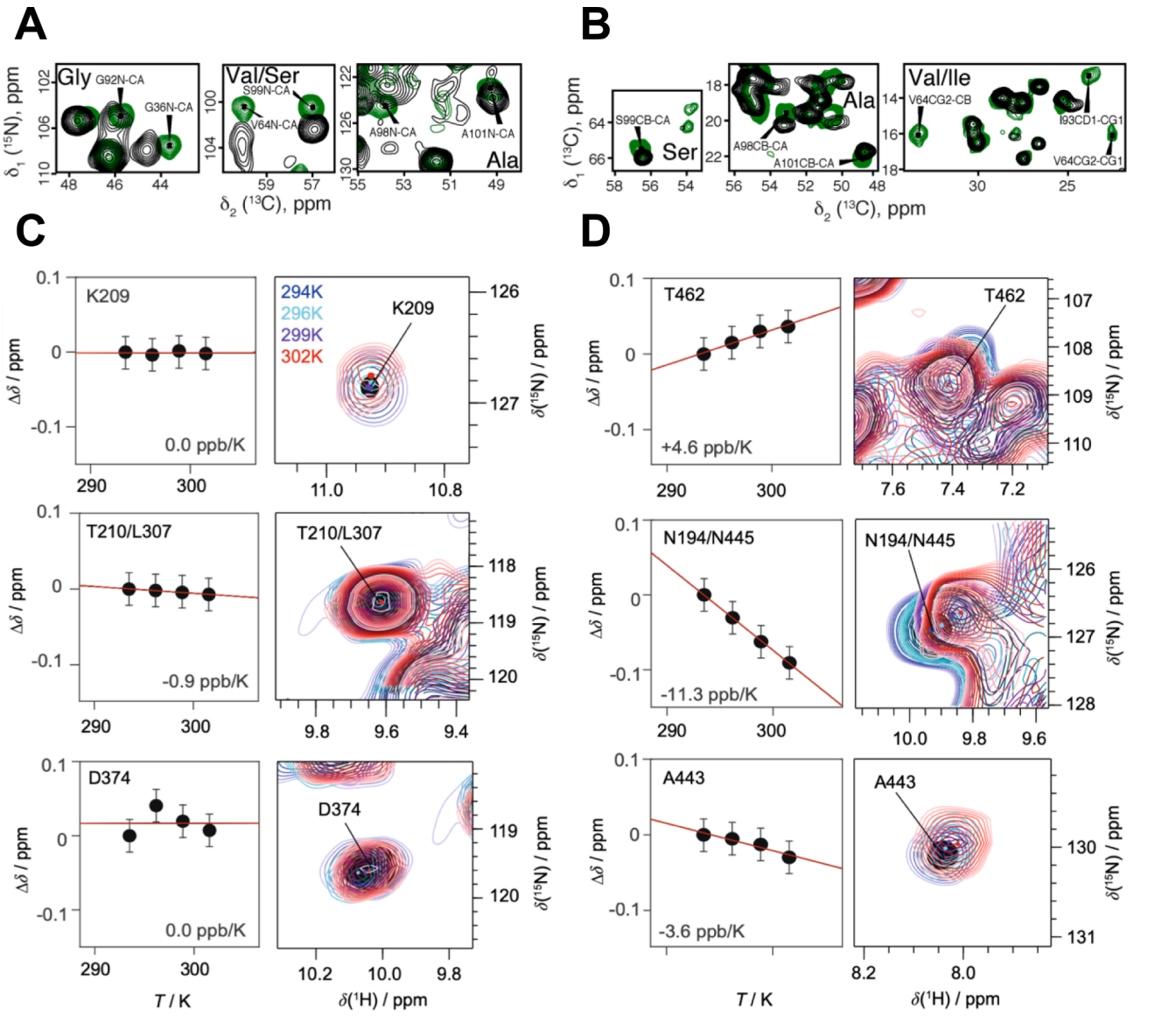

Fig. 3. CSP mapping to determine nucleic acid–protein binding interfaces in ssNMR. **(A)** Excerpts of overlaid 2D CP NCACX correlation spectra of free (black) and RNA-bound (green) *Pf* L7Ae protein, with peaks showing noticeable CSPs upon RNA binding. **(B)** Same as in **(C)** for 2D ^{13}C–^{13}C DARR correlation spectra. Figures **(A–B)** are reproduced from (Ahmed et al., 2020) ©2020 with permission from John Wiley and Sons. **(C–D)** Temperature-dependent proton chemical-shift perturbations. Residue-specific temperature coefficients and corresponding excerpts of the hNH spectra of DnaB helicase complexed with ADP:AlF_4 and ssDNA. Residues in **(C)** show nearly no dependence of their chemical shifts on temperature and are thus likely involved in hydrogen bonds. The chemical shifts of residues in **(D)** have a larger dependence on temperature and are thus not involved in hydrogen bonds. Figures **(C–D)** are reproduced from (Malär et al., 2021b) ©2021 with permission from Springer Nature.

Olsen et al., 2005, 2010), RNA as part of RNP complexes (Aguion et al., 2021; Ahmed et al., 2020; Marchanka et al., 2013, 2015, 2018b) and DNA–protein complexes (Boudet et al., 2019; Lacabanne et al., 2020; Malär et al., 2021b; Wiegand et al., 2020b, 2019,2017b,2016; Zehnder et al., 2021).

The main challenge in NMR of RNA both in solution and in solid-state is the overlap of the signals due to the limited chemical diversity of the nucleotides. This is especially true in canonical, and thus homogeneous, tertiary structure elements, such as A-form helices. This challenge can be addressed using nucleotide-type selective and/or segmental isotope labeling (Duss et al., 2010; Nelissen et al., 2008; Tzakos et al., 2007), as well as site-specific labeling (Lu et al., 2010; Marchanka et al., 2018a), which reduce spectral crowding. As mentioned above, selective labeling becomes crucial in ssNMR, where the signal overlaps are significant also for RNAs of medium size in the absence of significant structural diversity (i.e. in helical regions).

The second challenge in NMR of RNA is the unequal proton distribution. Nucleic acids have a high proton density in the ribose ring but only few protons in the nucleobases and no protons at the backbone phosphate. This leads to a limited number of ^{1}H–^{1}H distance restraints available to determine the conformation at both the backbone and the Watson-Crick and Hoogsteen sides of the nucleobases. Fortunately, in ssNMR, the number of distance restraints that can be collected does not directly correlate with the number of protons, as distance restraints can be measured via both heteronuclear and homonuclear correlations mediated by dipolar couplings. Moreover, the distance range of restraints measured in ssNMR experiments such as rotational echo double resonance (REDOR) (Gullion and Schaefer, 1989a, 1989b) or proton-driven spin diffusion (PDSD) (Szeverenyi et al., 1982) can exceed the range of those obtained in solution NMR by NOESY experiments (Huang et al., 2011, 2010; Marchanka and Carlomagno, 2019; Olsen et al., 2005, 2003; Studelska et al., 1996), providing a useful tool for the refinement

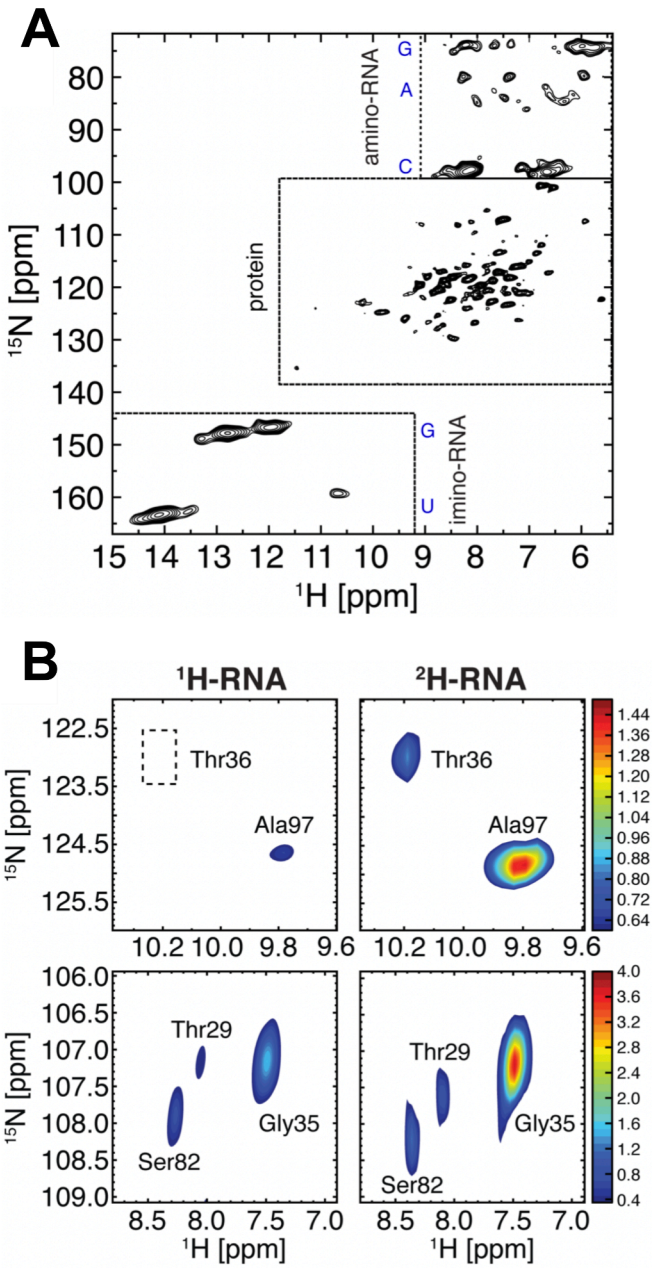

Fig. 4. Dipolar-coupling-mediated line broadening effects to probe intermolecular interactions. **(A)** 2D CP hNH correlation spectrum of ^{2}H,^{15}N labeled *Pf* L7Ae protein in complex with ^{2}H,^{13}C,^{15}N labeled 26mer Box C/D RNA (^{2}H-RNA), showing the characteristic protein and RNA spectral patterns. Labile protons were back exchanged to ^{1}H in a solution containing 10 %/90 % H_2O/D_2O. **(B)** Excerpts of 2D CP hNH spectra acquired on RNA–protein complexes containing either ^{13}C,^{15}N-labeled 26mer Box C/D RNA (^{1}H-RNA, left) or ^{2}H-RNA (right). The NMR peaks of protein residues near the RNA (Gly35, Thr36, and Ala97) are less intense in the spectrum of the sample containing ^{1}H-RNA, due to line broadening caused by the ^{1}H(protein)-^{1}H(RNA) dipolar couplings. Peaks from amide groups distant from the RNA hydrogens have similar intensities in the two samples (Thr29 and Ser82). Figures **(A–B)** are reproduced from (Asami et al., 2013) ©2013 with permission from John Wiley and Sons.

of global conformations. For example, REDOR experiments have provided long-range distance restraints up to 16 Å in proteins (Studelska et al., 1996) and 13 Å in nucleic acids (Olsen et al., 2003).

Because of its applicability to particles of large size and the versatility it offers in the design of magnetization transfer pathways, MAS ssNMR can adopt an important role in structural biology of RNP complexes. However, the disadvantages caused by signals overlap have long discouraged the application of ssNMR to RNA-containing particles. In the past decade our lab has developed a suite of ssNMR experiments that achieve assignment of RNA ^{13}C,^{15}N (Marchanka et al., 2015, 2013; Marchanka and Carlomagno, 2019) and ^{1}H resonances (Aguion et al., 2021; Aguion and Marchanka, 2021; Marchanka et al., 2018b) as well as *de novo* RNA structure determination using distance restraints obtained solely from ssNMR experiments (Marchanka et al., 2015). These experiments, together with those developed in several other laboratories for the structure determination of proteins using ^{13}C,^{15}N detection (Castellani et al., 2003; Zhao, 2012) at low MAS frequencies and ^{1}H detection (Andreas et al., 2016; Schubeis et al., 2018) at fast MAS frequencies (Penzel et al., 2019; Schledorn et al., 2020), allow the structure determination of the individual RNA and protein components of RNP complexes by ssNMR. Once the structures of the individual components are established, the identification of the intermolecular interfaces as well as the measurement of intermolecular distances yield the structure of the complex.

In this review we present recent advances of ssNMR spectroscopy to determine intermolecular contacts in RNP complexes and discuss advantages and challenges of the individual strategies. Due to the similar nature of the interfaces, we also review ssNMR studies of intermolecular interactions in DNA–protein complexes. We present conventional ssNMR methods that rely on the detection of low γ nuclei, such as ^{13}C, ^{15}N and ^{31}P, as well as novel ^{1}H-detected ssNMR experiments under fast magic-angle-spinning (MAS) rates. Finally, we discuss the first example of structure determination of an RNA–protein complex guided solely by ssNMR-derived restraints.

Sample preparation

NMR of nucleic acids is more challenging than that of proteins due to the poor chemical shift dispersion of their NMR signals. Thus, even for relatively small nucleic acids, advanced isotope labeling strategies may be required to obtain site specific structural information. Nucleic acids for ssNMR studies can be prepared by either chemical (Beaucage and Reese, 2009; Roy and Caruthers, 2013) or enzymatic synthesis; however, the methods available to produce isotope-labeled RNA are considerably more advanced than those available for DNA. An extensive description of isotope labeling strategies for RNA (Marchanka et al., 2018a) and ssDNA/dsDNA (Nelissen et al., 2016) by either chemical or enzymatic synthesis can be found in the literature.

As opposed to X-ray crystallography, ssNMR does not require crystals of any particular size and is therefore applicable to particles with substantial flexible regions, which are difficult to force in well-ordered, large crystals. Common sample preparation techniques in ssNMR include micro (nano)-crystallization (Bertini et al., 2010a; Franks et al., 2005; Huang et al., 2012; Marchanka et al., 2013; McDermott et al., 2000; Yang et al., 2017), ethanol precipitation (Zhao et al., 2019), lyophilization (Huang et al., 2011; Leppert et al., 2004; Olsen et al., 2008, 2005; Wang et al., 1994), freezing in the presence of a cryoprotectant (Siemer et al., 2012) or sedimentation of soluble macromolecules into the ssNMR rotor using ultracentrifugation (Barbet-Massin et al., 2015; Bertini et al., 2011; Gardiennet et al., 2012; Lacabanne et al., 2020; Wiegand et al., 2016, 2020a). Micro-crystallization, ethanol precipitation and sedimentation could all yield sufficiently narrow linewidths to allow for site-specific assignments in individual samples (Aguion and Marchanka, 2021); however, ethanol precipitation is incompatible with the protein component of RNP complexes, while sedimentation has been successfully applied to RNP complexes, such as the prokaryotic ribosome (Barbet-Massin et al., 2015), but no data is available with respect to RNA linewidths in these samples. In contrast, both lyophilization and flash-freezing have been demonstrated to lead to inhomogeneous line broadening (Huang et al., 2011; Olsen et al., 2005; Siemer et al., 2012), impairing site-specific assignments. Nevertheless, structural information can be obtained also for these samples, in

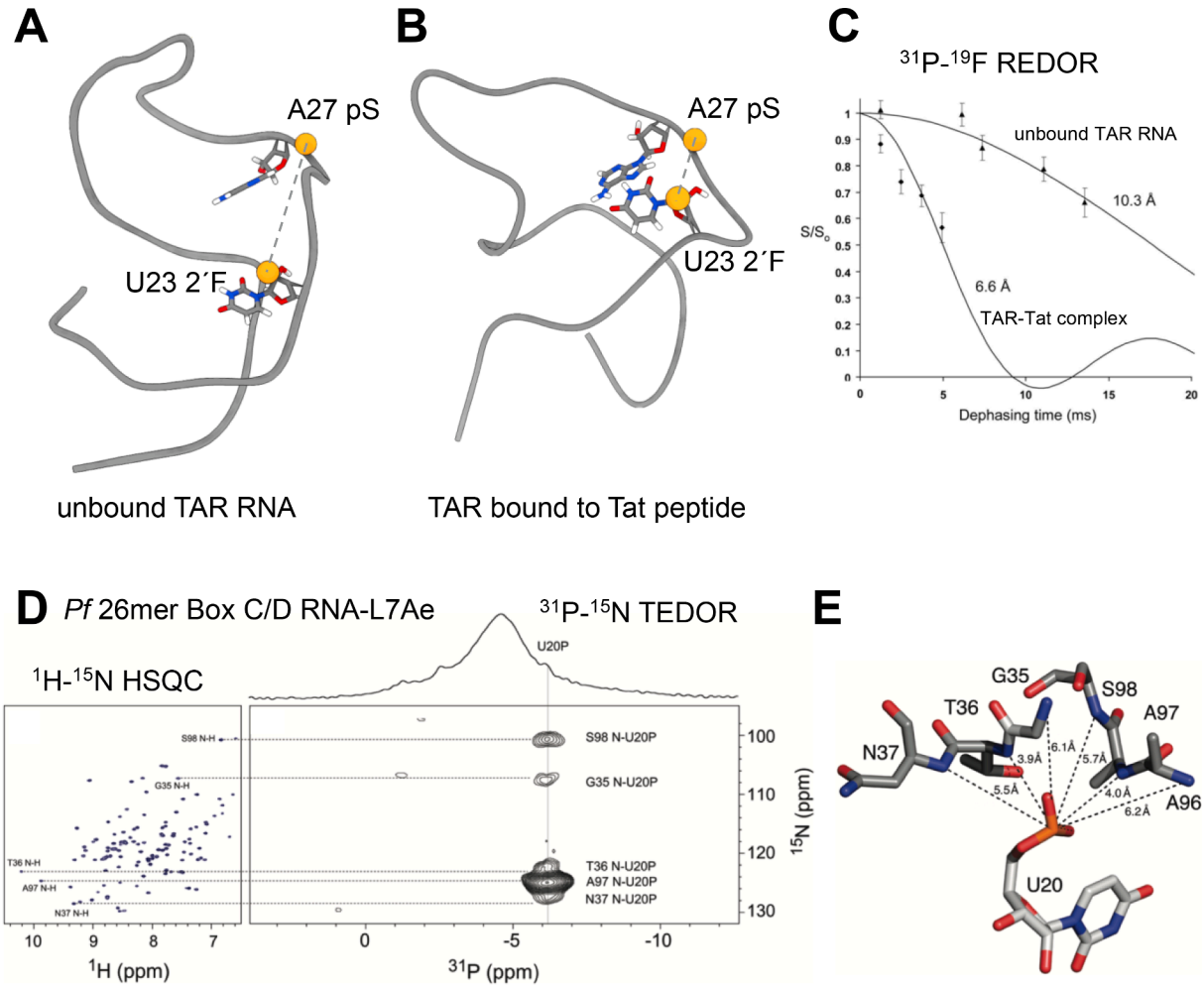

Fig. 5. Experiments utilizing TEDOR/REDOR recoupling to probe intermolecular contacts. **(A–C)** Conformational changes in TAR RNA upon binding to the Tat peptide. **(A)** Conformation of the free TAR RNA (PDB entry #1ANR). U: uridine; A: adenosine **(B)** Conformation of the TAR RNA bound to the Tat peptide (PDB entry #1ARJ). The RNA phosphate backbone is represented by a grey ribbon. Residues U23 and A27 are shown in sticks. Orange spheres mark the U23 2́-F and A27 pS positions. **(C)** ^{31}P-^{19}F REDOR dephasing curves for free TAR RNA (triangle) and the TAR RNA–Tat peptide complex (rhombus). Solid lines represent simulated dephasing curves corresponding to an internuclei distance of 10.3 Å in the free TAR RNA and 6.6 Å in the TAR RNA–Tat peptide complex. Figures **(A–C)** are adapted from (Olsen et al., 2005) ©2005 with permission from Oxford University Press. **(D–E)** Intermolecular cross-peaks between the *Pf* 26mer Box C/D and L7Ae. **(D)** Left, solution ^{1}H-^{15}N HSQC spectrum of the *Pf* L7Ae protein bound to Box C/D RNA. Right, ^{31}P-^{15}N TEDOR spectrum showing cross-peaks between the amide ^{15}N nuclei of the ^{15}N-labelled L7Ae protein and the ^{31}P nuclei of the unlabeled Box C/D RNA. Dashed lines from the left to the right panel connect peaks with the same ^{15}N chemical shift. A: alanine; G: glycine; N: asparagine; S: serine; T: threonine. **(E)** Intermolecular distances between the L7Ae backbone ^{15}N nuclei and the U20 ^{31}P nucleus of the Box C/D RNA measured with the ^{31}P-^{15}N TEDOR experiment in **(D)**. Figures **(D–E)** are reproduced from (Jehle et al., 2010) ©2010 with permission from American Chemical Society.

combination with site-specific isotopic labeling (Huang et al., 2011, 2010; Olsen et al., 2005).

ssNMR of nucleic acid–protein complexes prepared using either sedimentation or micro-crystallization have been reported to be stable over a long time. A DNA–protein–ATP complex prepared by sedimentation and stored at –20 °C for 3 years has been shown to yield virtually the same ^{13}C–^{13}C DARR spectrum as the freshly prepared sample (Lacabanne et al., 2020; Wiegand et al., 2020a). A ssNMR RNP complex sample prepared by micro-crystallization in our laboratory (Aguion et al., 2021) shows identical ^{1}H–^{13}C and ^{1}H-^{15}N fingerprint spectra after storage at + 4 °C for two years, with only minimal loss of signal intensities (Fig. 1).

Finally, ssNMR ^{1}H-detected experiments at MAS rates above 100 kHz require low sample quantities (300–800 µg for rotors of 0.7–0.8-mm size) (Aguion et al., 2021; Lacabanne et al., 2020; Marchanka et al., 2018b), thus limiting the cost and time-demand of sample preparation.

Characterization of nucleic acid–protein interfaces by MAS ssNMR

The approaches used so far to characterize intermolecular contacts in nucleic acid–protein complexes can be divided in three classes, whereby many of the published studies use a combination of these approaches.

(i) Similar to solution-state NMR, the involvement of a molecular surface in interactions with a binding partner can be detected by either chemical shift perturbations (CSPs) or intensity changes of the ssNMR peaks of the surface atoms, when comparing the free and the bound-state of the molecule (Ahmed et al., 2020; Boudet et al., 2019; Lacabanne et al., 2020; Malär et al., 2021b; Wiegand et al., 2020b, 2019,2016; Williamson, 2013). For example, the formation of an hydrogen bond at a nucleic acid–protein interface causes a downfield shift of the involved ^{1}H atom (Wagner et al., 1983). Changes in peak intensities can report on changes in the dynamics of one of the binding partners upon complex formation

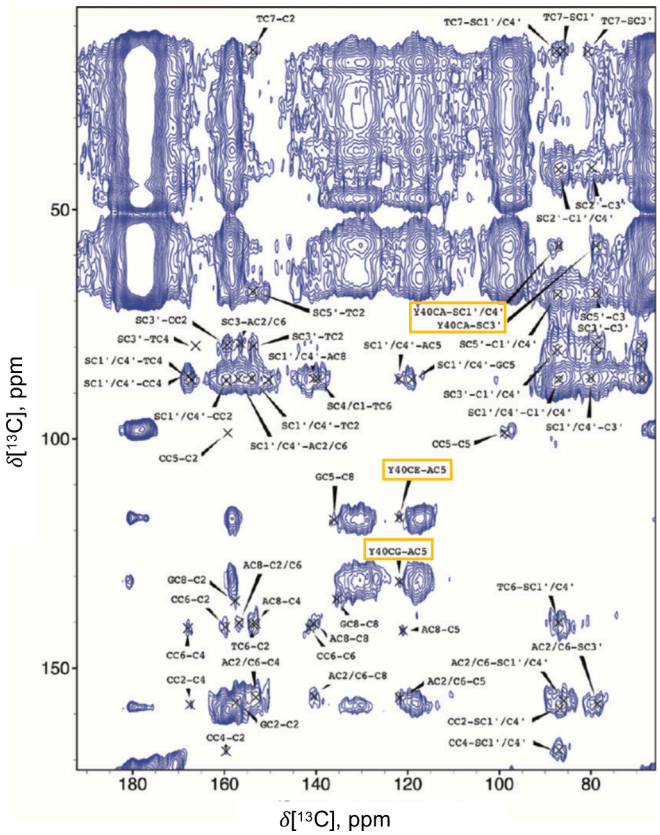

Fig. 6. Homonuclear 2D ^{13}C–^{13}C DARR spectrum of uniformly ^{13}C,^{15}N-labeled Pf1 bacteriophage virion. The spectrum shows cross peaks between the ssDNA ribose and base atoms and a specific tyrosine residue (Y40) of the viral coat protein, as highlighted by orange boxes. The figure is reproduced from (Sergeyev et al., 2011) ©2011 with permission from American Chemical Society.

(Lacabanne et al., 2020; Wiegand et al., 2019). In another study, Asami et al. measured a ^{15}N-^{1}H correlation spectrum of a protein in complex with either ^{1}H or ^{2}H-RNA (Asami et al., 2013) and quantified the difference in protein peaks' intensities that distinguished the RNA–protein interface, owing to the line-broadening caused by the RNA ^{1}H in the ^{1}H-RNA–protein complex. These effects are specific to the surface of the protein in contact with the RNA, while CSPs can also occur in regions other than the intermolecular surface, due to allosteric effects. In any case, both CSPs and changes in peak intensities can be used as ambiguous restraints in docking protocols.

(ii) Intermolecular distances can be measured directly through intermolecular dipolar correlation experiments. In solution-state NMR, intermolecular distances are measured through ^{13}C,^{15}N-edited, ^{12}C,^{14}N-filtered ^{1}H–^{1}H NOESY experiments (Breeze, 2000; Zwahlen et al., 1997). In ssNMR, a plethora of methods yield dipolar correlations, such as cross-polarization (CP) (Hartmann and Hahn, 1962), rotational echo double resonance (REDOR) (Gullion and Schaefer, 1989a, 1989b) and the closely related transferred echo double resonance (TEDOR) (Hing et al., 1992), as well as dipolar-assisted rotational resonance (DARR) (Takegoshi et al., 2001, 1999), proton-driven spin diffusion (PDSD) (Szeverenyi et al., 1982), proton spin diffusion (PSD) (Lange et al., 2002; Wilhelm et al., 1998), radio frequency-driven dipolar recoupling (RFDR) (Bennett et al., 1992; Sodickson et al., 1993), or combined $R2^{v}_{n}$-driven (CORD) (Hou et al., 2013) experiments. One of the most popular approaches for the measurement of nucleic acid–protein distances utilizes TEDOR-based ^{31}P–^{13}C and and ^{31}P–^{15}N correlations (Bechinger et al., 2011; Huang et al., 2011, 2010; Jehle et al., 2010; Olsen et al., 2005; Yu and Schaefer, 2008). ^{31}P has a high gyromagnetic ratio (Table 1) and is present in nucleic acids exclusively and with 100 % isotopic abundance; thus, in the presence of a ^{13}C,^{15}N-labeled protein, these correlation experiments are sensitive and report exclusively on intermolecular contacts between the protein and the nucleic acid.

(iii) The third approach utilizes paramagnetic relaxation enhancement (PRE) effects, which rely on the interaction between nuclei and unpaired electrons. Because the electron spin gyromagnetic ratio is approximately 600-times larger than that of the ^{1}H nucleus, these effects are large and can be used to measure longer distances than internuclear dipolar correlations. In solution, PRE measurements have been often applied to measure long-range intra- and intermolecular distances (up to 30 Å) in nucleic acid–protein complexes (Amrane et al., 2014; Graziadei et al., 2020; Hennig et al., 2015; Lapinaite et al., 2013; Leeper et al., 2010; MacKereth et al., 2011; Martin-Tumasz et al., 2010). For a detailed description of paramagnetic NMR in solution and solid-state, readers are referred to a comprehensive review by Pell and coworkers (Pell et al., 2019). In ssNMR, PRE measurements were first employed to identify residues of metalloproteins in proximity to the paramagnetic metal (Balayssac et al., 2007b, 2007a; Pintacuda et al., 2007); recently, PRE experiments have also been used to study nucleic acid–protein complexes, (Ahmed et al., 2020; Wiegand et al., 2017a; Zehnder et al., 2021). Notably, Ahmed et al. report the first structure of an RNP complex obtained solely from ssNMR data.

Fig. 2 gives an overview of the methods developed and utilized to date to probe nucleic acid–protein interfaces, which will be discussed in detail in the next chapters. A representative set of ssNMR studies of nucleic acid–protein complexes is given in Table 2 in chronological order.

Chemical shift perturbations and intensity changes

Both CSPs and peak intensities changes can be used to reveal intermolecular surfaces. CSP mapping can be achieved with all types of NMR spectra. In ^{13}C,^{15}N-detected ssNMR, chemical-shift differences measured in 2D ^{13}C–^{13}C DARR spectra (Ahmed et al., 2020; Boudet et al., 2019; Wiegand et al., 2016, 2019) and 2D CP ^{13}C,^{15}N spectra (Ahmed et al., 2020; Boudet et al., 2019; Wiegand et al., 2019) of ^{13}C,^{15}N-labeled proteins in the free and complexed forms were used to identify surfaces involved in nucleic-acid binding (Fig. 3A–B). Wiegand et al. used 1D ^{1}H-^{31}P CP spectra to detect binding of a protein to $(dT)_{20}$ ssDNA, whose ^{31}P peaks shifted from ~ –1 ppm in the free form to 0–1 ppm in the protein-bound form (Wiegand et al., 2016, 2019). However, nucleic acid CSPs have never been used to reveal the nucleic acid residues involved in protein recognition. This task is indeed challenging, especially for RNAs, as these do not always adopt a single conformation in the free form and thus the observed CSPs may report on both folding and binding.

Recently, ^{1}H-detected ssNMR methods, such as CP hNH and hCH experiments (Zhou et al., 2007a, 2007b; Zhou and Rienstra, 2008), have been utilized to map CSPs of a ^{13}C,^{15}N labeled protein in a DNA–protein complex upon nucleotide binding to yield a DNA–protein–nucleotide complex (Lacabanne et al., 2020; Wiegand et al., 2020b). ^{1}H-detection in MAS ssNMR is expected to greatly enhance the resolution and sensitivity of CSP mapping.

Another chemical-shift-based approach was developed by Malär et al. to detect protein side chains involved in hydrogen bonds with the nucleic acid and the nucleotide in a ssDNA–protein–nucleotide complex (Malär et al., 2021b). The method measures the temperature dependence of ^{1}H chemical shifts and correlates a weak dependence with the involvement of the ^{1}H in a hydrogen bond. This correlation was often

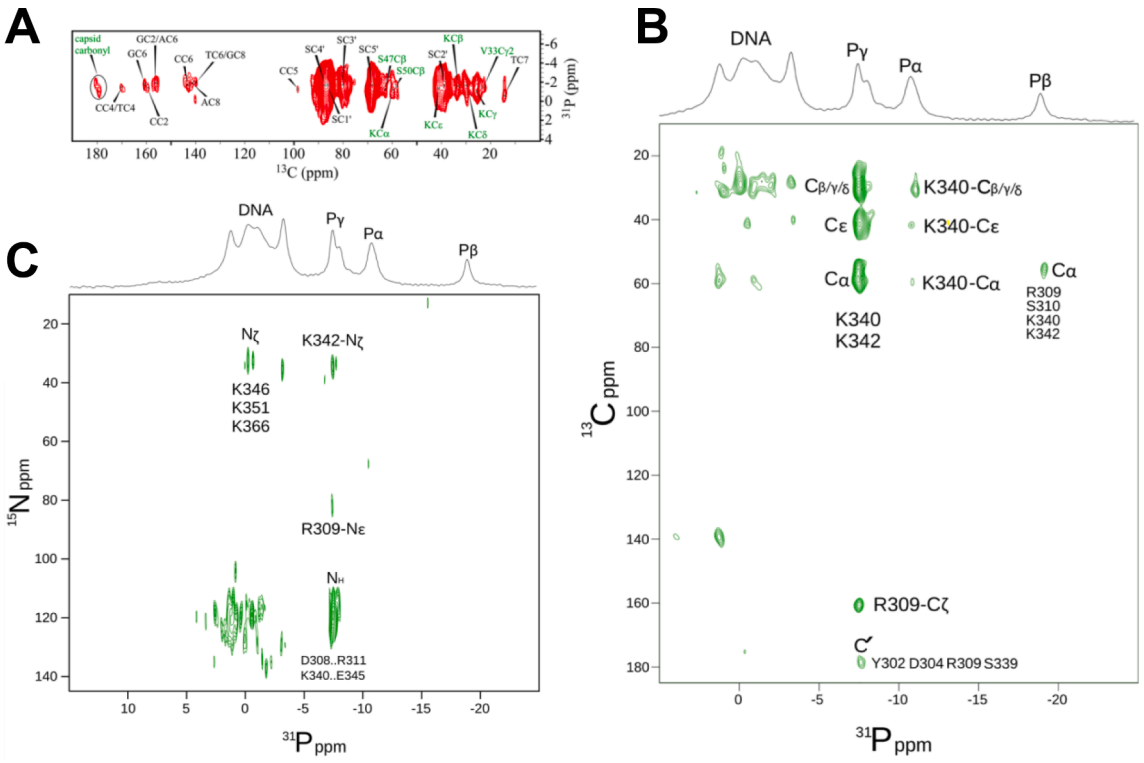

Fig. 7. ^{1}H–^{1}H PSD-based experiments to probe intermolecular contacts. **(A)** 2D PHHC correlation spectrum of intact fd bacteriophage to probe intermolecular interactions between DNA phosphate and protein carbon atoms. fd bacteriophages were prepared on a ^{13}C,^{15}N enriched medium supplemented with non-isotopically labeled aromatic amino acid precursors to obtain particles with uniformly ^{13}C,^{15}N labeled DNA and selectively unlabeled proteins. The figure is reproduced from (Morag et al., 2014) ©2014 with permission from American Chemical Society. **(B–C)** Intermolecular correlations between uniformly ^{13}C,^{15}N-labeled pRN1 archaeal primase and a 9 nt functional DNA sequence, as well as bound ATP. **(B)** 2D CHHP correlation spectrum. **(C)** 2D NHHP correlation spectrum. Figures **(B–C)** are reproduced from (Boudet et al., 2019) ©2019 with permission from Elsevier.

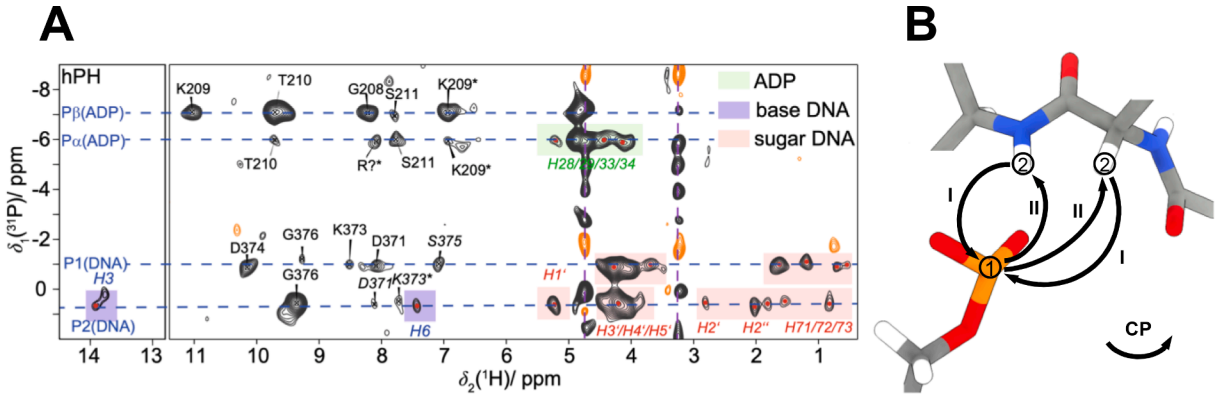

Fig. 8. CP-based hPH experiment to probe intermolecular contacts. **(A)** 2D CP-based hPH correlation spectrum of uniformly ^{13}C,^{15}N-labeled DnaB helicase in complex with ADP:AlF_4 and ssDNA. Intramolecular correlations of phosphate groups with ADP protons are highlighted in green; intramolecular correlations of phosphate groups with DNA protons are highlighted in light purple and red. The remaining peaks are assigned to intermolecular correlations of phosphate groups with amide backbone protons, except for those indicated by an asterisk, which are associated with sidechain protons. The figure is reproduced from (Malär et al., 2021b) ©2021 with permission from Springer Nature. **(B)** Magnetization transfer scheme of the 2D hPH experiment exemplarily shown for a phosphate group in close contact with the amide backbone. Encircled numbers indicate the chemical-shift evolution times corresponding to the two spectral dimensions, and the roman numerals indicate the CP transfer periods.

demonstrated in solution (Baxter and Williamson, 1997; Cierpicki et al., 2002; Cierpicki and Otlewski, 2001) and more recently also in ssNMR (Malär et al., 2021a). Mapping the dependence of chemical shifts on temperature in a CP hNH experiment, Malär et al. were able to confirm that the chemical shifts of ^{1}H protein atoms previously identified as forming hydrogen bonds with the nucleotide and the DNA vary very little with temperature and certainly much less than those not involved in hydrogen bonds (Fig. 3C–D). These experiments, when applied to proteins in both the free and nucleic acid-bound states, can reveal which protein amino acids are involved in nucleic acid recognition.

The first study that employed quantification of ssNMR peak intensities to determine intermolecular surfaces in an RNP complex was communicated by Asami et al. (Asami et al., 2013), who also pioneered ^{1}H-detection in MAS ssNMR of uniformly ^{13}C,^{15}N labeled RNA at moderate MAS frequencies of 20 kHz. The ^{1}H-^{15}N cross peaks of protein and RNA detected in a hNH experiment (Zhou et al., 2007a, 2007b; Zhou

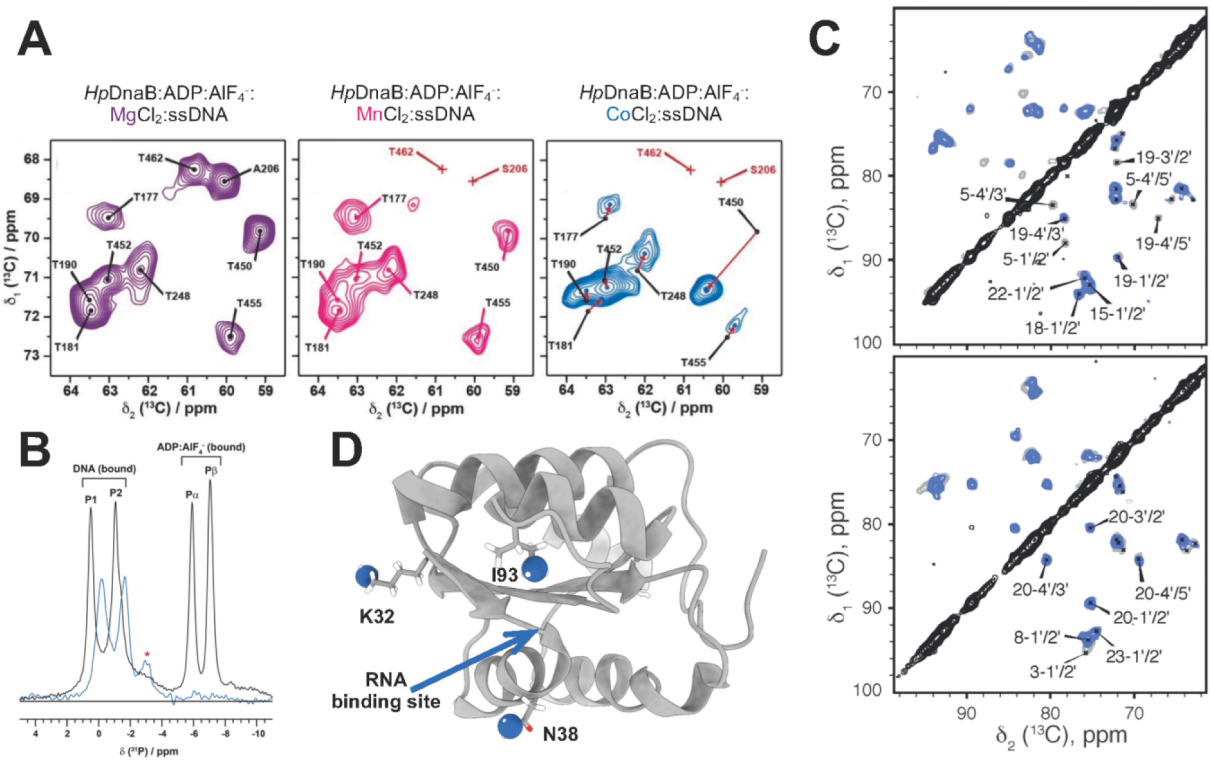

Fig. 9. Paramagnetic effects in ssNMR of nucleic acid–protein complexes. **(A)** Threonine region of ^{13}C–^{13}C correlation spectra of DnaB helicase in complex with ADP:AlF_4 and ssDNA in the presence of Mg^{2+} (purple), paramagnetic Mn^{2+} (pink) and paramagnetic Co^{2+} (blue). Peaks which are no longer visible in the paramagnetic spectra, due to PRE effects, are marked with red crosses. Changes in chemical shifts (PCS) are highlighted by red arrows in the sample with Co^{2+}. **(B)** 1D ^{1}H-^{31}P CPMAS NMR of the ssDNA–DnaB–ADP:AlF_4 complex in the presence of either Mg^{2+} (black) or Co^{2+} (blue). Figures **(A–B)** are reproduced from (Malär et al., 2021b) ©2021 with permission from John Wiley and Sons. **(C)** Overlay of 2D ^{13}C,^{13}C SPC-5 correlation spectra of A^{lab} 26mer Box C/D RNA (top panel) and U^{lab} 26mer Box C/D RNA (bottom panel) in complex with nitroxide-tagged L7Ae-K32C protein in the diamagnetic (grey) and paramagnetic (blue) state. Peaks of residues in proximity to the paramagnetic tag have reduced signal intensities in the paramagnetic state. **(D)** Ribbon representation of the L7Ae protein (PDB entry #6TPH) showing the residues selected for coupling with the paramagnetic tag (K32, N38 and I93) represented as blue spheres. Figures **(C–D)** are adapted from (Ahmed et al., 2020) ©2020 with permission from John Wiley and Sons.

and Rienstra, 2008) do not significantly overlap, with the exception of those belonging to RNA amino groups and protein arginine sidechains (Fig. 4A). This allowed monitoring both components of the complex simultaneously. To obtain narrow linewidths in the hNH experiment at low MAS speed, both RNA and protein were ^{2}H,^{15}N labeled and the labile ^{2}H were back-exchanged to ^{1}H to a 10 % extent. To identify the surface of the protein that binds the RNA, Asami et al. measured protein ^{1}H-^{15}N correlations of two samples, containing ^{2}H,^{15}N-labeled protein and either ^{2}H,^{13}C,^{15}N-labeled RNA or ^{13}C,^{15}N-labeled RNA. By comparing the intensities of the ^{1}H-^{15}N protein cross peaks in the two samples they could identify which protein amino acids form the RNA–protein interface, as the ^{1}H-^{15}N peaks of these amino acids had reduced intensities in the sample containing non-deuterated RNA, due to the line broadening of the protein H_Ns caused by the dipolar interaction with the nearby RNA ^{1}H atoms. Spectra simulations using the program SIMPSON (Bak et al., 2000) demonstrated that a measurable effect occurred when the distance between the protein H_N and any RNA hydrogen was less than 6–8 Å, while the intensities of the protein amide peaks further than 8 Å from the RNA were identical in the two spectra (Fig. 4B). In principle, the ratio of signal intensities in the two samples can be quantified and converted in a distance value; however, as the experiment does not reveal which RNA hydrogen causes the line broadening of a given protein H_N, these distances cannot be used as unambiguous restraints in structure calculations.

Other studies detected side-chain-specific nucleic acid–protein interactions by monitoring the appearance or disappearance of arginine and lysine side chain peaks in ^{15}N-^{13}C CP correlation spectra or CP hNH spectra upon binding of either nucleic acids or nucleotides (Lacabanne et al., 2020; Wiegand et al., 2019). The appearance of the peaks of these side chains was due to the loss of local dynamics connected with binding. Wiegand et al. also detected the appearance of a ^{31}P-^{31}P correlation peak in the ^{31}P-^{31}P DARR spectrum of the $(dT)_{20}$ ssDNA upon binding to the DnaB–ADP:AlF_4 binary complex, as a result of the rigidification of two of the 20 ssDNA nucleotides when they formed the ssDNA–protein–nucleotide complex (Wiegand et al., 2020b).

Cross-interface dipolar correlations

MAS ssNMR techniques to measure internuclear distances were first applied to an RNA–peptide complex by Olsen et al., who, however, did not measure intermolecular distances but detected peptide binding through the change in the value of a ^{19}F-^{31}P distance in the RNA (Olsen et al., 2005). The ^{19}F atom was introduced as a 2′-fluorine at an individual site, while the ^{31}P belonged to a single phosphorothioate (pS) label in the RNA backbone and thus could be easily assigned (Fig. 5A–B). The distance was measured in a ^{31}P-^{19}F REDOR experiment (Gullion and Schaefer, 1989a, 1989b; Merritt et al., 1999) (Fig. 5C). Distance measurements between two unique sites were used before to detect binding in a DNA–protein complex (Yu et al., 2004) and in DNA–small molecule complexes (Mehta et al., 2004; Olsen et al., 2003). The introduction of fluorine atoms at individual position in nucleic acids, either in the ribose as 2′-F, or in the base, as 5-fluorouridine (5FU) and 5-fluorocytidine (5FC), has become popular because of the large chemical shift dispersion of ^{19}F and the high sensitivity of its chemical shift to the structural and chemical environment (Hennig et al., 2007; Marchanka et al., 2018a; Scott et al., 2004). Moreover, substitution of ^{1}H by ^{19}F in nucleic

Fig. 10. Overlay of the MD-refined ssNMR structure (blue) (PDB entry #6TPH) of the *Pf* Box C/D RNA–L7Ae complex with the crystallographic structure of the orthologous Box C/D RNA–L7Ae complex from *Archaeoglobus fulgidus* (*Af*) (gold) (PDB entry #4BW0) (Huang and Lilley, 2013). The figure is reproduced from (Ahmed et al., 2020) ©2020 with permission from John Wiley and Sons.

acids has a negligible effect on both structure (Hennig et al., 2007; Merritt et al., 1999) and intermolecular interactions (Olsen et al., 2005).

The substitution of an individual phosphate group with a thiophosphate has also been widely used in NMR spectroscopy of nucleic acids to unambiguously identify individual ^{31}P atoms thanks to the downfield shift by 50–60 ppm induced by the sulfur atom on the ^{31}P chemical shift (Huang et al., 2011, 2010; Merritt et al., 1999; Olsen et al., 2005, 2003). Also in this case, the pS substitution results in little-to-no perturbation to the global structure, as demonstrated by several high-resolution NMR studies for DNA:RNA hybrids (Bachelin et al., 1998; González et al., 1995; Merritt et al., 1999) and crystal structures of wild-type and pS-substituted DNA duplexes (Cruse et al., 1986). However, alterations of RNA conformation caused by pS substitutions have been reported as well (Smith and Nikonowicz, 2000). In addition, the different charge distribution and polarizability of thiophosphate in comparison to phosphate alters the strength of both ionic interactions and hydrogen bonds and thus, potentially, nucleic acid–protein affinities (Milligan and Uhlenbeck, 1989; Schnitzer and Von Ahsen, 1997). Consequently, it is safer to use methods that do not require chemical modification of the nucleic acid to measure internuclear distances in the context of nucleic acid–protein complexes. With the recent developments in the ssNMR experimental design and sample preparation techniques, it is nowadays possible to obtain site-specific assignments of ^{31}P resonances in the backbone of ^{13}C,^{15}N labeled RNA by, for example, ^{13}C-^{31}P-TEDOR and ^{13}C-^{31}P-TEDOR-^{13}C–^{13}C-PDSD experiments (Marchanka et al., 2015; Marchanka and Carlomagno, 2019). In addition, ^{1}H-detected hPH experiments serve as useful complement to confirm ^{31}P resonance assignments (Malär et al., 2021b).

^{13}C-^{31}P, ^{15}N-^{31}P, ^{13}C-^{19}F and ^{15}N-^{19}F REDOR experiments on an RNA–peptide complex (Huang et al., 2011, 2010), as well as ^{31}P-^{15}N TEDOR experiments on an RNA–protein complex (Jehle et al., 2010) were used to measure the first intermolecular RNA–peptide and RNA–-protein distances through the dipolar coupling between the RNA ^{19}F and ^{31}P nuclei and the protein/peptide ^{13}C and ^{15}N nuclei (Fig. 5D–E). These experiments were performed on complexes containing ^{13}C,^{15}N-labeled protein and unlabeled or selectively fluorinated RNA and yielded exclusively intermolecular cross peaks. Huang et al. utilized a selectively labeled peptide, where a single arginine was ^{13}C,^{15}N enriched, and 5FU/pS-modified RNA (Huang et al., 2011, 2010). Besides the problems discussed above with regards to the impact of chemical modifications on RNA structure and interactions, the use of selectively labeled molecules requires these molecules to be available by chemical synthesis, to allow the easy incorporation of labeled or modified building blocks at any position in the primary sequence. This requirement limits the applicability of the strategy. In a more general approach, Jehle et al. measured ^{31}P-^{15}N RNA backbone-protein backbone distances between a uniformly ^{13}C,^{15}N labeled protein and an unlabeled RNA (Jehle et al., 2010). As the assignment of both ^{31}P RNA (Marchanka et al., 2015; Marchanka and Carlomagno, 2019) and ^{15}N protein (Andreas et al., 2016; Castellani et al., 2003; Schubeis et al., 2018; Zhao, 2012) peaks can be obtained by ssNMR experiments, the method is broadly applicable.

Other studies used ^{15}N-^{31}P REDOR experiments to probe intermolecular contacts between either bacteriophage T4 DNA or salmon sperm DNA ^{31}P atoms and ^{15}N atoms of lysine side chains in either a DNA–-protein (Yu and Schaefer, 2008) or a DNA–peptide complex (Bechinger et al., 2011). In both cases, the interacting atoms were not assigned, and the experiments were used solely to prove binding.

Following a different approach, Sergeyev et al. (Sergeyev et al., 2011) were able to detect cross-peaks between the uniformly ^{13}C,^{15}N labeled ssDNA of the Pf1 bacteriophage virion and a specific tyrosine residue of the viral coat protein using dynamic nuclear polarization (DNP) enhanced homonuclear ^{13}C–^{13}C DARR correlation experiments (Abragam and Goldman, 1978; Akbey and Oschkinat, 2016; Su et al., 2015; Takegoshi et al., 2001, 1999). The aromatic stacking interactions between the DNA bases and the tyrosine had been previously predicted but had remained unproven, until they were detected by ssNMR (Fig. 6).

In another study (Morag et al., 2014), fd bacteriophages were prepared on a ^{13}C,^{15}N enriched medium supplemented with non-isotopically labeled aromatic amino acid precursors to obtain particles with uniformly labeled DNA and selectively-unlabeled proteins. Assignment of atom-types of the fd bacteriophage circular ssDNA was obtained using a ^{13}C–^{13}C CORD correlation experiment (Hou et al., 2013). However, due to the large size of the DNA, site-specific resonance assignment was not attempted. The contacts between the ssDNA and the virion capsid proteins were measured in ^{13}C–^{13}C CORD and ^{13}C–^{13}C DARR experiments. The intermolecular correlations could be distinguished from the intramolecular ones due to the partially different chemical shift ranges of ^{13}C atoms in DNA and proteins. DNA phosphate-capsid protein interactions were detected utilizing homonuclear ^{1}H–^{1}H PSD mixing (Lange et al., 2002; Wilhelm et al., 1998) coupled with P—H and H—C CP transfers (Hartmann and Hahn, 1962) in a PHHC experiment. The PHHC experiment yielded intramolecular correlations between the DNA phosphate backbone and ^{13}C nuclei of the DNA riboses and bases as well as intermolecular correlations between the DNA phosphate backbone and side chains of amino acids of the coat protein, in particular lysines (Fig. 7A). This study is remarkable, due to the large size of the particles under investigation. A similar approach could be used to reveal RNA–protein interfaces in RNP complexes, possibly in combination with site-specific assignments. However, neither ^{13}C–^{13}C DARR nor PHHC experiments have been applied to measure RNA-protein distances so far.

The CHHP experiment, which is conceptually the same as the PHHC experiment, but with detection of ^{13}C and ^{31}P chemical shifts in t_1 and t_2, respectively, and the NHHP experiment, where polarization is transferred between the protein ^{15}N nuclei and the DNA ^{31}P nuclei through ^{1}H–^{1}H spin diffusion, were utilized in other studies (Boudet et al., 2019; Wiegand et al., 2019, 2020b) to observe intermolecular ^{13}C-^{31}P and ^{15}N-^{31}P contacts between a ^{13}C,^{15}N-labeled protein and DNA (Fig. 7B, C).

All these ^{31}P-^{13}C/^{15}N heteronuclear correlation experiments suffer

from low signal-to-noise ratio (SNR), in particular for large complexes. The problem can be addressed using DNP, which can significantly enhance the SNR of NMR spectra exploiting the transfer of the large electron polarization to nuclear spins. However, biomolecular MAS-DNP studies are typically performed at cryogenic temperatures, which lead to significant broadening of the NMR lines (Bauer et al., 2017; Siemer et al., 2012; Siemer and McDermott, 2008). Nevertheless, in DNP-enhanced ^{31}P-^{13}C CP and PHHC transfer experiments, Wiegand et al. measured intermolecular contacts between a ^{13}C,^{15}N labeled protein and either ssDNA or ADP in a ssDNA–protein–ADP complex (Wiegand et al., 2017b). In both cases, a ^{13}C–^{13}C DARR mixing step was added after the intermolecular transfer step to reduce spectral overlap, resulting in 2D ^{13}C,^{13}C (P)C—C and (ii) 2D (PHH)C—C correlation spectra. Due to the line broadening induced by cryogenic temperatures, the experiments yielded information only on the protein amino-acid type in contact with either ADP or ssDNA, but allowed neither site-specific protein assignments nor discrimination between the ^{31}P chemical shifts of the ssDNA and ADP. Of note, the ^{1}H–^{1}H spin-diffusion-driven PHHC-C correlation is less selective than the direct CP-driven PC-C correlation but can yield longer ^{31}P-^{13}C distances of the order of 7–10 Å.

Finally, Malär et al. have recently probed spatial proximities between protein ^{1}H nuclei and nucleic acid/nucleotide ^{31}P nuclei in a ssDNA–protein–ADP complex utilizing a ^{1}H-detected ^{13}P-^{1}H correlation experiment under high MAS speed of 105 kHz (Fig. 8) (Malär et al., 2021b). The CP hPH experiment can be performed with unlabeled material and appears to be much more sensitive for probing spatial proximity of hydrogen atoms to phosphate groups than the previously described ^{1}H–^{1}H PSD-based CHHP and NHHP experiments.

Paramagnetic relaxation enhancement

The first implementation of PREs in ssNMR of a protein–nucleotide complex took advantage of the fact that ATP-binding is often accompanied by binding of Mg^{2+} ions, which can be substituted by paramagnetic ions such as Mn^{2+} (Bonneau and Legault, 2014; Tamaki et al., 2016) and Co^{2+} (Balayssac et al., 2008; Bertini et al., 2010b) without affecting protein function (Otting, 2010). The presence of a paramagnetic center can cause an increase of the relaxation rates (paramagnetic relaxation enhancement, PRE) and/or a change in the chemical shifts (pseudo-contact shifts, PCS) of close-by nuclei (Jaroniec, 2012). These effects dependent quantitatively on the distance between the nucleus and the paramagnetic center. Through the analysis of signal intensities in 2D ^{13}C,^{13}C DARR spectra of the diamagnetic (in the presence of Mg^{2+}) and paramagnetic (in the presence of Mn^{2+}) protein–nucleotide complex, Wiegand et al. identified protein residues close to the nucleotide binding site (Wiegand et al., 2017a). Recently, Zehnder et al. extended this approach to a ssDNA–protein–nucleotide complex, in which Mn^{2+} and Co^{2+} ions were used as paramagnetic centers (Zehnder et al., 2021). 2D ^{13}C,^{13}C DARR, as well as 2D NCA and 3D NCACB spectra (Baldus et al., 1998) were recorded for diamagnetic and paramagnetic ssDNA–protein–nucleotide complexes (Fig. 9A) to localize the metal ion in the complex. Moreover, PCSs of the $(dT)_{20}$ ssDNA observed in 1D ^{1}H-^{31}P CP spectra allowed to localize the DNA phosphate groups in the complex (Fig. 9B).

If the molecule of interest does not have a well-defined, individual metal binding site, paramagnetic centers can be introduced in nucleic acid–protein complexes by coupling nitroxide-based tags, one-by-one, to individual cysteine residues engineered at specific protein sites (Nadaud et al., 2007). The PRE effects caused by the paramagnetic tag on the RNA can be used to measure RNA–protein distances in the RNP complex (Ahmed et al., 2020). Ahmed et al. measured PRE effects induced in an RNP complex by protein-coupled paramagnetic tags on ^{13}C,^{15}N-labeled RNA in 2D ^{13}C,^{13}C SPC-5 correlation spectra (Hohwy et al., 2002, 1999) (Fig. 9C). Unlike CSPs, which are sensitive also to allosteric effects, PRE-effects are specific reporters of intermolecular contacts. To avoid PRE effects generated by interparticle contacts in the precipitate, the paramagnetic-labeled RNP complex was diluted in 1:3 molar ratio with the diamagnetic, unlabeled RNP complex.

To obtain enough RNA-protein distance restraints by this methodology, the paramagnetic tag should be placed close to the RNA binding site but in such way as not to affect binding (Fig. 9D). CSP data, discussed previously, can guide in the recognition of the RNA binding surface and in the design of the cysteine mutants. The integrity of the complex, after introduction of the nitroxide tag, should be verified by careful inspection of the NMR spectra and of other biophysical properties of the complex. As far as nucleic acids are concerned, paramagnetic tags can be covalently attached to either the phosphate backbone or the ribose or modified bases. In alternative, modified paramagnetic nucleotides can be introduced into the RNA by solid-phase synthesis (Miao et al., 2021). Although paramagnetically tagged RNA has not been used in ssNMR so far, these techniques can be easily applied to increase the number of paramagnetic sites that can be probed in nucleic acid–protein complexes.

Structure determination of an RNP complex by ssNMR only

Ahmed et al. succeeded in determining the structure of the complex formed by the *Pf* protein L7Ae and the 26mer Box C/D RNA using exclusively ssNMR-derived restraints (Ahmed et al., 2020). They achieved this goal through a docking protocol, which started from the individual structures of protein-bound 26mer RNA determined by ssNMR (Marchanka et al., 2015) and RNA-bound L7Ae protein (Xue et al., 2010). The RNA-bound protein structure was determined by X-ray crystallography, but in principle it would have been accessible by ssNMR through well-established methodology (Schubeis et al., 2018; Zhao, 2012). The docking protocol was implemented in the program Haddock (Dominguez et al., 2003) and used a combination of ssNMR-derived CSP and PRE data to guide complex assembly.

PRE-based restraints were derived from the quantification of PRE effects observed on nucleotide-type specific ^{13}C,^{15}N labeled (A^{lab} and U^{lab}) RNA in 2D ^{13}C,^{13}C SPC-5 spectra and induced by 3 different paramagnetic tags coupled to the unlabeled protein. PRE effects were quantified as peak volume ratios in spectra measured for the same sample in either the paramagnetic (with the nitroxide radical coupled to a cysteine residue) or the diamagnetic state (after addition of ascorbic acid to reduce the radical). These ratios (V^{para}/V^{dia}) were converted into distance restraints in a semi-quantitative manner, whereby the intramolecular V^{para}/V^{dia} ratios of the protein peaks, whose electron-nucleus distances were known from the protein structure, were used to calibrate a linear regression between the V^{para}/V^{dia} ratio and the electron-nucleus distance. Although not rigorously correct, this linear regression, with the appropriate tolerance bounds, was good enough to deliver broad distance ranges that defined the relative position of the protein and the RNA to a good level of precision.

CSP-derived ambiguous restraints were measured for the protein in 2D ^{13}C–^{13}C DARR and 2D CP ^{13}C,^{15}N spectra of uniformly ^{13}C,^{15}N labeled protein in the free and RNA-bound states.

In total 72 restraints were used for the docking and lead a 26mer Box C/D RNA–L7Ae structure that is very similar to that of an orthologous Box C/D RNA–L7Ae complex determined by crystallography, thus verifying the accuracy of the ssNMR-derived structure (Fig. 10). This exemplary study demonstrates the ability of ssNMR to yield nucleic acid–protein complex structures at atomic resolution.

Conclusions and outlook

The ssNMR methods discussed here build a suite of complementary experiments that identify interaction interfaces and yield intermolecular distance restraints in nucleic acid–protein complexes. They provide a powerful tool to determine the structural basis of intermolecular recognition for those nucleic acids–protein complexes that are not

amenable to X-ray crystallography, cryo-EM or solution-state NMR. The structure of the individual components of the complex can be obtained by ssNMR as well as with previously published and often reviewed methodology (Marchanka and Carlomagno, 2019; Schubeis et al., 2018; Zhao, 2012).

In 2021 the program AlphaFold (Jumper et al., 2021) revolutionized structural biology of folded protein domains and their complexes, by demonstrating an unprecedented accuracy in the prediction of protein folding and interactions based on database knowledge. Nucleic acid structures, in particular RNA, are difficult to predict, as they largely depend on the environment and on the binding partners. Thus, it is unclear whether AlphaFold will ever be expanded to this class of polymers. In view of this, NMR spectroscopy, with its power to illuminate intermolecular interactions involving flexible molecules, gains unique relevance.

To date, many studies of nucleic acid–protein complexes have focused on obtaining site specific information for the proteins in the complex. The nucleic acid component has been often neglected due to lack of spectral resolution and limited access to advanced isotope labeling techniques. In the past few years, the ssNMR toolkit for studying nucleic acids and their complexes has grown steadily, including both technical developments in MAS ssNMR and isotope labeling techniques. Consequently, we expect MAS ssNMR of nucleic acid–protein complexes to rapidly grow in relevance and scope, including site specific structural information on both the protein and nucleic acid components of the complex.

Declaration of Competing Interest

The authors declare that they have no known competing financial interests or personal relationships that could have appeared to influence the work reported in this paper.

Acknowledgements

This work has received support from the DFG (Deutsche Forschungsgemeinschaft) grant CA294/21-1 to T.C.

References

Abragam, A., Goldman, M., 1978. Principles of dynamic nuclear polarisation. Reports Prog. Phys. 41, 395–467. https://doi.org/10.1088/0034-4885/41/3/002.

Abramov, G., Velyvis, A., Rennella, E., Wong, L.E., Kay, L.E., 2020. A methyl-TROSY approach for NMR studies of high-molecular-weight DNA with application to the nucleosome core particle. Proc. Natl. Acad. Sci. U. S. A. 117, 12836–12846. https://doi.org/10.1073/pnas.2004317117.

Aguion, P.I., Kirkpatrick, J., Carlomagno, T., Marchanka, A., 2021. Identification of RNA Base Pairs and Complete Assignment of Nucleobase Resonances by Proton-Detected Solid-State NMR Spectroscopy at 100 kHz MAS. Angew. Chem. Int. Ed. 60, 23903–23910. https://doi.org/10.1002/anie.202107263.

Aguion, P.I., Marchanka, A., 2021. Strategies for RNA Resonance Assignment by 13C/15N- and 1H-Detected Solid-State NMR Spectroscopy. Front. Mol. Biosci. 8, 1–16. https://doi.org/10.3389/fmolb.2021.743181.

Ahmed, M., Marchanka, A., Carlomagno, T., 2020. Structure of a Protein–RNA Complex by Solid-State NMR Spectroscopy. Angew. Chem. Int. Ed. 59, 6866–6873. https://doi.org/10.1002/anie.201915465.

Akbey, Ü., Oschkinat, H., 2016. Structural biology applications of solid state MAS DNP NMR. J. Magn. Reson. 269, 213–224. https://doi.org/10.1016/j.jmr.2016.04.003.

Amrane, S., Rebora, K., Zniber, I., Dupuy, D., Mackereth, C.D., 2014. Backbone-independent nucleic acid binding by splicing factor SUP-12 reveals key aspects of molecular recognition. Nat. Commun. 5 https://doi.org/10.1038/ncomms5595.

Andreas, L.B., Jaudzems, K., Stanek, J., Lalli, D., Bertarelloa, A., Marchand, T.L., De Paepe, D.C., Kotelovica, S., Akopjana, I., Knott, B., Wegner, S., Engelke, F., Lesage, A., Emsley, L., Tars, K., Herrmann, T., Pintacuda, G., 2016. Structure of fully protonated proteins by proton-detected magic- Angle spinning NMR. Proc. Natl. Acad. Sci. U. S. A. 113, 9187–9192. https://doi.org/10.1073/pnas.1602248113.

Asami, S., Rakwalska-Bange, M., Carlomagno, T., Reif, B., 2013. Protein-RNA interfaces probed by 1H-detected MAS solid-state NMR spectroscopy. Angew. Chem. Int. Ed. 52, 2345–2349. https://doi.org/10.1002/anie.201208024.

Bachelin, M., Hessler, G., Kurz, G., Hacia, J.G., Dervan, P.B., Kessler, H., 1998. Structure of a stereoregular phosphorothioate DNA/RNA duplex. Nat. Struct. Biol. 5, 271–276.

Bak, M., Rasmussen, J.T., Nielsen, N.C., 2000. SIMPSON: A General Simulation Program for Solid-State NMR Spectroscopy. J. Magn. Reson. 147, 296–330. https://doi.org/10.1006/jmre.2000.2179.

Balayssac, S., Bertini, I., Fälber, K., Fragai, M., Jehle, S., Lelli, M., Luchinat, C., Oschkinat, H., Kwon, J.Y., 2007a. Solid-state NMR of matrix metalloproteinase 12: An approach complementary to solution NMR. ChemBioChem 8, 486–489. https://doi.org/10.1002/cbic.200600408.

Balayssac, S., Bertini, I., Lelli, M., Luchinat, C., Maletta, M., 2007b. Paramagnetic ions provide structural restraints in solid-state NMR of proteins. J. Am. Chem. Soc. 129, 2218–2219. https://doi.org/10.1021/ja068105a.

Balayssac, S., Bertini, I., Bhaumik, A., Lelli, M., Luchinat, C., 2008. Paramagnetic shifts in solid-state NMR of proteins to elicit structural information. Proc. Natl. Acad. Sci. U. S. A. 105, 17284–17289. https://doi.org/10.1073/pnas.0708460105.

Baldus, M., Petkova, A.T., Herzfeld, J., Griffin, R.G., 1998. Cross polarization in the tilted frame: Assignment and spectral simplification in heteronuclear spin systems. Mol. Phys. 95, 1197–1207. https://doi.org/10.1080/00268979809483251.

Barbet-Massin, E., Huang, C.T., Daebel, V., Hsu, S.T.D., Reif, B., 2015. Site-specific solid-state NMR studies of "trigger factor" in complex with the large ribosomal subunit 50S. Angew. Chem. Int. Ed. 54, 4367–4369. https://doi.org/10.1002/anie.201409393.

Bauer, T., Dotta, C., Balacescu, L., Gath, J., Hunkeler, A., Böckmann, A., Meier, B.H., 2017. Line-Broadening in Low-Temperature Solid-State NMR Spectra of Fibrils. J. Biomol. NMR 67, 51–61. https://doi.org/10.1007/s10858-016-0083-4.

Baxter, N.J., Williamson, M.P., 1997. Temperature dependence of 1H chemical shifts in proteins. J. Biomol. NMR 9, 359–369. https://doi.org/10.1023/A:1018334207887.

Beaucage, S.L., Reese, C.B., 2009. Recent advances in the chemical synthesis of RNA. Current Protocols in Nucleic Acid Chemistry. https://doi.org/10.1002/0471142700.nc0216s38.

Bechinger, B., Vidovic, V., Bertani, P., Kichler, A., 2011. A new family of peptide-nucleic acid nanostructures with potent transfection activities. J. Pept. Sci. 17, 88–93. https://doi.org/10.1002/psc.1318.

Bennett, A.E., Ok, J.H., Griffin, R.G., Vega, S., 1992. Chemical shift correlation spectroscopy in rotating solids: Radio frequency-driven dipolar recoupling and longitudinal exchange. J. Chem. Phys. 96, 8624–8627. https://doi.org/10.1063/1.462267.

Ben-Shem, A., Garreau de Loubresse, N., Melnikov, S., Jenner, L., Yusupova;Gulnara, Yusupov, M., 2011. The Structure of the Eukaryotic Ribosome at 3.0 Å Resolution. Science. 334, 1524–1529.

Bertini, I., Bhaumik, A., De Paëpe, G., Griffin, R.G., Lelli, M., Lewandowski, J.R., Luchinat, C., 2010a. High-resolution solid-state NMR structure of a 17.6 kDa protein. J. Am. Chem. Soc. 132, 1032–1040. https://doi.org/10.1021/ja906426p.

Bertini, I., Emsley, L., Lelli, M., Luchinat, C., Mao, J., Pintacuda, G., 2010b. Ultrafast MAS solid-state NMR permits extensive 13C and 1H detection in paramagnetic metalloproteins. J. Am. Chem. Soc. 132, 5558–5559. https://doi.org/10.1021/ja100398q.

Bertini, I., Luchinat, C., Parigi, G., Ravera, E., Reif, B., Turano, P., 2011. Solid-state NMR of proteins sedimented by ultracentrifugation. Proc. Natl. Acad. Sci. U. S. A. 108, 10396–10399. https://doi.org/10.1073/pnas.1103854108.

Blanco, F.J., Montoya, G., 2011. Transient DNA/RNA-protein interactions. FEBS J. 278, 1643–1650. https://doi.org/10.1111/j.1742-4658.2011.08095.x.

Bonneau, E., Legault, P., 2014. NMR localization of divalent cations at the active site of the neurospora VS ribozyme provides insights into RNA-metal-ion interactions. Biochemistry 53, 579–590. https://doi.org/10.1021/bi401484a.

Boudet, J., Devillier, J.C., Wiegand, T., Salmon, L., Meier, B.H., Lipps, G., Allain, F.H.T., 2019. A Small Helical Bundle Prepares Primer Synthesis by Binding Two Nucleotides that Enhance Sequence-Specific Recognition of the DNA Template. Cell 176, 154–166.e13. https://doi.org/10.1016/j.cell.2018.11.031.

Breeze, A.L., 2000. Isotope-filtered NMR methods for the study of biomolecular structure and interactions. Prog. Nucl. Magn. Reson. Spectrosc. 36, 323–372. https://doi.org/10.1016/S0079-6565(00)00020-0.

Brown, J.D., Kharytonchyk, S., Chaudry, I., Iyer, A.S., Carter, H., Becker, G., Desai, Y., Glang, L., Choi, S.H., Singh, K., Lopresti, M.W., Orellana, M., Rodriguez, T., Oboh, U., Hijji, J., Ghinger, F.G., Stewart, K., Francis, D., Edwards, B., Chen, P., Case, D.A., Telesnitsky, A., Summers, M.F., 2020. Structural basis for transcriptional start site control of HIV-1 RNA fate. Science 368, 413–417. https://doi.org/10.1126/science.aaz7959.

Cady, S.D., Schmidt-Rohr, K., Wang, J., Soto, C.S., Degrado, W.F., Hong, M., 2010. Structure of the amantadine binding site of influenza M2 proton channels in lipid bilayers. Nature 463, 689–692. https://doi.org/10.1038/nature08722.

Campagne, S., Gervais, V., Milon, A., 2011. Nuclear magnetic resonance analysis of protein-DNA interactions. J. R. Soc. Interface 8, 1065–1078. https://doi.org/10.1098/rsif.2010.0543.

Carlomagno, T., 2014. Present and future of NMR for RNA-protein complexes: A perspective of integrated structural biology. J. Magn. Reson. 241, 126–136. https://doi.org/10.1016/j.jmr.2013.10.007.

Castellani, F., Van Rossum, B.J., Diehl, A., Rehbein, K., Oschkinat, H., 2003. Determination of solid-state NMR structures of proteins by means of three-dimensional 15N–13C-13C dipolar correlation spectroscopy and chemical shift analysis. Biochemistry 42, 11476–11483. https://doi.org/10.1021/bi034903r.

Cech, T.R., Steitz, J.A., 2014. The noncoding RNA revolution - Trashing old rules to forge new ones. Cell 157, 77–94. https://doi.org/10.1016/j.cell.2014.03.008.

Choy, J.S., Wei, S., Lee, J.Y., Tan, S., Chu, S., Lee, T.H., 2010. DNA methylation increases nucleosome compaction and rigidity. J. Am. Chem. Soc. 132, 1782–1783. https://doi.org/10.1021/ja910264z.

Cierpicki, T., Otlewski, J., 2001. Amide proton temperature coefficients as hydrogen bond indicators in proteins. J. Biomol. NMR 21, 249–261. https://doi.org/10.1023/A:1012911329730.

Cierpicki, T., Zhukov, I., Byrd, R.A., Otlewski, J., 2002. Hydrogen bonds in human ubiquitin reflected in temperature coefficients of amide protons. J. Magn. Reson. 157, 178–180. https://doi.org/10.1006/jmre.2002.2597.

Colvin, M.T., Silvers, R., Ni, Q.Z., Can, T.V., Sergeyev, I., Rosay, M., Donovan, K.J., Michael, B., Wall, J., Linse, S., Griffin, R.G., 2016. Atomic Resolution Structure of Monomorphic Aβ42 Amyloid Fibrils. J. Am. Chem. Soc. 138, 9663–9674. https://doi.org/10.1021/jacs.6b05129.

Corley, M., Burns, M.C., Yeo, G.W., 2020. How RNA-Binding Proteins Interact with RNA: Molecules and Mechanisms. Mol. Cell 78, 9–29. https://doi.org/10.1016/j.molcel.2020.03.011.

Cruse, W.B.T., Salisbury, S.A., Brown, T., Cosstick, R., Eckstein, F., Kennard, O., 1986. Chiral phosphorothioate analogues of B-DNA. The crystal structure of Rp-d|Gp(S)CpGp(S)CpGp(S)C|. J. Mol. Biol. 192, 891–905. https://doi.org/10.1016/0022-2836(86)90035-5.

Dominguez, C., Boelens, R., Bonvin, A.M.J.J., 2003. HADDOCK: A protein-protein docking approach based on biochemical or biophysical information. J. Am. Chem. Soc. 125, 1731–1737. https://doi.org/10.1021/ja026939x.

Dominguez, C., Schubert, M., Duss, O., Ravindranathan, S., Allain, F.H.T., 2011. Structure determination and dynamics of protein-RNA complexes by NMR spectroscopy. Prog. Nucl. Magn. Reson. Spectrosc. 58, 1–61. https://doi.org/10.1016/j.pnmrs.2010.10.001.

Duss, O., Maris, C., Von Schroetter, C., Allain, F.H.T., 2010. A fast, efficient and sequence-independent method for flexible multiple segmental isotope labeling of RNA using ribozyme and RNase H cleavage. Nucleic Acids Res. 38, e188 https://doi.org/10.1093/nar/gkq756.

Franks, W.T., Zhou, D.H., Wylie, B.J., Money, B.G., Graesser, D.T., Frericks, H.L., Sahota, G., Rienstra, C.M., 2005. Magic-angle spinning solid-state NMR spectroscopy of the β1 immunoglobulin binding domain of protein G (GB1): 15N and 13C chemical shift assignments and conformational analysis. J. Am. Chem. Soc. 127, 12291–12305. https://doi.org/10.1021/ja044497e.

Gardiennet, C., Schütz, A.K., Hunkeler, A., Kunert, B., Terradot, L., Böckmann, A., Meier, B.H., 2012. A sedimented sample of a 59 kDa dodecameric helicase yields high-resolution solid-state NMR spectra. Angew. Chem. Int. Ed. 51, 7855–7858. https://doi.org/10.1002/anie.201200779.

Ghanim, G.E., Fountain, A.J., van Roon, A.M.M., Rangan, R., Das, R., Collins, K., Nguyen, T.H.D., 2021. Structure of human telomerase holoenzyme with bound telomeric DNA. Nature 593, 449–453. https://doi.org/10.1038/s41586-021-03415-4.

Goldbourt, A., Gross, B.J., Day, L.A., McDermott, A.E., 2007. Filamentous phage studied by magic-angle spinning NMR: Resonance assignment and secondary structure of the coat protein in Pf1. J. Am. Chem. Soc. 129, 2338–2344. https://doi.org/10.1021/ja066928u.

González, C., James, T.L., Stec, W., Reynolds, M.A., 1995. Structure and Dynamics of a DNARNA Hybrid Duplex with a Chiral Phosphorothioate Moiety: NMR and Molecular Dynamics with Conventional and Time-Averaged Restraints. Biochemistry 34, 4969–4982. https://doi.org/10.1021/bi00015a008.

Graziadei, A., Gabel, F., Kirkpatrick, J.P., Carlomagno, T. 2020 The guide sRNA sequence determines the activity level of Box C/D RNPs eLife 2020 9:e50027 https://doi.org/10.7554/eLife.50027.

Gullion, T., Schaefer, J., 1989a. Rotational-Echo Double-Resonance NMR. J. Magn. Reson. 81, 196–200. https://doi.org/10.1016/j.ssnmr.2010.07.002.

Gullion, T., Schaefer, J., 1989b. Detection of Weak Heteronuclear Dipolar Coupling by Rotational-Echo Double-Resonance Nuclear Magnetic Resonance. Adv. Magn. Opt. Reson. https://doi.org/10.1016/B978-0-12-025513-9.50009-4.

Hartmann, S.R., Hahn, E.L., 1962. Nuclear double resonance in the rotating frame. Phys. Rev. 128, 2042–2053. https://doi.org/10.1103/PhysRev.128.2042.

Helm, M., 2006. Post-transcriptional nucleotide modification and alternative folding of RNA. Nucleic Acids Res. 34, 721–733. https://doi.org/10.1093/nar/gkj471.

Hennig, J., Warner, L.R., Simon, B., Geerlof, A., Mackereth, C.D., Sattler, M., 2015. Structural analysis of protein-RNA complexes in solution using NMR paramagnetic relaxation enhancements, 1st ed, Methods in Enzymology. Elsevier Inc. https://doi.org/10.1016/bs.mie.2015.02.006.

Hennig, M., Scott, L.G., Sperling, E., Bermel, W., Williamson, J.R., 2007. Synthesis of 5-fluoropyrimidine nucleotides as sensitive NMR probes of RNA structure. J. Am. Chem. Soc. 129, 14911–14921. https://doi.org/10.1021/ja073825i.

Hing, A.W., Vega, S., Schaefer, J., 1992. Transferred-echo double-resonance NMR. J. Magn. Reson. 96, 205–209. https://doi.org/10.1016/0022-2364(92)90305-Q.

Hohwy, M., Rienstra, C.M., Jaroniec, C.P., Griffin, R.G., 1999. Fivefold symmetric homonuclear dipolar recoupling in rotating solids: Application to double quantum spectroscopy. J. Chem. Phys. 110, 7983–7992. https://doi.org/10.1063/1.478702.

Hohwy, M., Rienstra, C.M., Griffin, R.G., 2002. Band-selective homonuclear dipolar recoupling in rotating solids. J. Chem. Phys. 117, 4973–4987. https://doi.org/10.1063/1.1488136.

Hoop, C.L., Lin, H.K., Kar, K., Magyarfalvi, G., Lamley, J.M., Boatz, J.C., Mandal, A., Lewandowski, J.R., Wetzel, R., Van Der Wel, P.C.A., 2016. Huntingtin exon 1 fibrils feature an interdigitated β-hairpin-based polyglutamine core. Proc. Natl. Acad. Sci. U. S. A. 113, 1546–1551. https://doi.org/10.1073/pnas.1521933113.

Hou, G., Yan, S., Trebosc, J., Amoureux, J.-P., Polenova, T., 2013. Broadband Homonuclear Correlation Spectroscopy Driven by Combined R2 nv Sequences under Fast Magic Angle Spinning for NMR Structural Analysis of Organic and Biological Solids. J. Magn. Reson. 232, 18–30. https://doi.org/10.1016/j.jmr.2013.04.009. Broadband.

Huang, W., Varani, G., Drobny, G.P., 2010. 13C/15N-19F intermolecular REDOR NMR study of the interaction of TAR RNA with tat peptides. J. Am. Chem. Soc. 132, 17643–17645. https://doi.org/10.1021/ja1051439.

Huang, W., Varani, G., Drobny, G.P., 2011. Interactions of protein side chains with RNA defined with REDOR solid state NMR. J. Biomol. NMR 51, 347–356. https://doi.org/10.1007/s10858-011-9573-6.

Huang, W., Bardaro, M.F., Varani, G., Drobny, G.P., 2012. Preparation of RNA samples with narrow line widths for solid state NMR investigations. J. Magn. Reson. 223, 51–54. https://doi.org/10.1016/j.jmr.2012.07.018.

Huang, W., Emani, P.S., Varani, G., Drobny, G.P., 2017. Ultraslow Domain Motions in HIV-1 TAR RNA revealed by solid-state deuterium NMR. J. Phys. Chem. B 121, 110–117. https://doi.org/10.1021/acs.jpcb.6b11041.

Huang, L., Lilley, D.M.J., 2013. The molecular recognition of kink-turn structure by the L7Ae class of proteins. RNA 19, 1703–1710. https://doi.org/10.1261/rna.041517.113.

Jackson, R.N., Golden, S.M., van Erp, P.B.G., Carter, J., Westra, E.R., Brouns, S.J.J., van der Oost, J., Terwilliger, T.C., Read, R.J., Wiedenheft, B., 2014. Structural biology. Crystal structure of the CRISPR RNA-guided surveillance complex from Escherichia coli. Science 345, 1473–1479. https://doi.org/10.1126/science.1256328.

Jaroniec, C.P., 2012. Solid-state nuclear magnetic resonance structural studies of proteins using paramagnetic probes. Solid State Nucl. Magn. Reson. 43–44, 1–13. https://doi.org/10.1016/j.ssnmr.2012.02.007.

Jehle, S., Falb, M., Kirkpatrick, J.P., Oschkinat, H., Van Rossum, B.J., Althoff, G., Carlomagno, T., 2010. Intermolecular protein-RNA interactions revealed by 2D31P-15N magic angle spinning solid-state NMR spectroscopy. J. Am. Chem. Soc. 132, 3842–3846. https://doi.org/10.1021/ja909723f.

Jumper, J., Evans, R., Pritzel, A., et al., 2021. Highly accurate protein structure prediction with AlphaFold. Nature 596, 583–589. https://doi.org/10.1038/s41586-021-03819-2.

Kawai, G., Yamamoto, Y., Watanabe, T., Yokoyama, S., Kamimura, T., Masegi, T., Sekine, M., Hata, T., Iimori, T., Miyazawa, T., 1992. Conformational Rigidity of Specific Pyrimidine Residues in tRNA Arises from Posttranscriptional Modifications That Enhance Steric Interaction between the Base and the 2'-Hydroxyl Group. Biochemistry 31, 1040–1046. https://doi.org/10.1021/bi00119a012.

Kay, L.E., 2011. Solution NMR spectroscopy of supra-molecular systems, why bother? A methyl-TROSY view. J. Magn. Reson. 210, 159–170. https://doi.org/10.1016/j.jmr.2011.03.008.

Keane, S.C., Heng, X., Lu, K., Kharytonchyk, S., Ramakrishnan, V., Carter, G., Barton, S., Hosic, A., Florwick, A., Santos, J., Bolden, N.C., McCowin, S., Case, D.A., Johnson, B. A., Salemi, M., Telesnitsky, A., Summers, M.F., 2015. Structure of the HIV-1 RNA packaging signal. Science 348, 917–921. https://doi.org/10.1126/science.aaa9266.

Khatter, H., Myasnikov, A.G., Natchiar, S.K., Klaholz, B.P., 2015. Structure of the human 80S ribosome. Nature 520, 640–645. https://doi.org/10.1038/nature14427.

Lacabanne, D., Boudet, J., Malär, A.A., Wu, P., Cadalbert, R., Salmon, L., Allain, F.H.T., Meier, B.H., Wiegand, T., 2020. Protein Side-Chain-DNA Contacts Probed by Fast Magic-Angle Spinning NMR. J. Phys. Chem. B 124, 11089–11097. https://doi.org/10.1021/acs.jpcb.0c08150.

Lange, A., Luca, S., Baldus, M., 2002. Structural constraints from proton-mediated rare-spin correlation spectroscopy in rotating solids. J. Am. Chem. Soc. 124, 9704–9705. https://doi.org/10.1021/ja026691b.

Lange, A., Giller, K., Hornig, S., Martin-Eauclaire, M.F., Pongs, O., Becker, S., Baldus, M., 2006. Toxin-induced conformational changes in a potassium channel revealed by solid-state NMR. Nature 440, 959–962. https://doi.org/10.1038/nature04649.

Lapinaite, A., Simon, B., Skjaerven, L., Rakwalska-Bange, M., Gabel, F., Carlomagno, T., 2013. The structure of the box C/D enzyme reveals regulation of RNA methylation. Nature 502, 519–523. https://doi.org/10.1038/nature12581.

Leeper, T.C., Qu, X., Lu, C., Moore, C., Varani, G., 2010. Novel protein-protein contacts facilitate mRNA 3'-processing signal recognition by Rna15 and Hrp1. J. Mol. Biol. 401, 334–349. https://doi.org/10.1016/j.jmb.2010.06.032.

Leppert, J., Urbinati, C.R., Häfner, S., Ohlenschläger, O., Swanson, M.S., Görlach, M., Ramachandran, R., 2004. Identification of NH...N hydrogen bonds by magic angle spinning solid state NMR in a double-stranded RNA associated with myotonic dystrophy. Nucleic Acids Res. 32, 1177–1183. https://doi.org/10.1093/nar/gkh288.

Lu, K., Miyazaki, Y., Summers, M.F., 2010. Isotope labeling strategies for NMR studies of RNA. J. Biomol. NMR 46, 113–125. https://doi.org/10.1007/s10858-009-9375-2.

Lusky, O.S., Meir, M., Goldbourt, A., 2021. Characterizing hydrogen bonds in intact RNA from MS2 bacteriophage using magic angle spinning NMR. Biophys. Reports 1, 100027. https://doi.org/10.1016/j.bpr.2021.100027.

MacKereth, C.D., Madl, T., Bonnal, S., Simon, B., Zanier, K., Gasch, A., Rybin, V., Valcárcel, J., Sattler, M., 2011. Multi-domain conformational selection underlies pre-mRNA splicing regulation by U2AF. Nature 475, 408–413. https://doi.org/10.1038/nature10171.

Malär, A.A., Völker, L.A., Cadalbert, R., Lecoq, L., Ernst, M., Böckmann, A., Meier, B.H., Wiegand, T., 2021a. Temperature-Dependent Solid-State NMR Proton Chemical-Shift Values and Hydrogen Bonding. J. Phys. Chem. B 125, 6222–6230. https://doi.org/10.1021/acs.jpcb.1c04061.

Malär, A.A., Wili, N., Völker, L.A., Kozlova, M.I., Cadalbert, R., Däpp, A., Weber, M.E., Zehnder, J., Jeschke, G., Eckert, H., Böckmann, A., Klose, D., Mulkidjanian, A.Y., Meier, B.H., Wiegand, T., 2021b. Spectroscopic glimpses of the transition state of ATP hydrolysis trapped in a bacterial DnaB helicase. Nat. Commun. 12, 1–13. https://doi.org/10.1038/s41467-021-25599-z.

Marchanka, A., Carlomagno, T., 2019. Solid-State NMR Spectroscopy of RNA, 1st ed, Methods in Enzymology. Elsevier Inc. https://doi.org/10.1016/bs.mie.2018.08.029.

Marchanka, A., Simon, B., Carlomagno, T., 2013. A suite of solid-state NMR experiments for RNA intranucleotide resonance assignment in a 21 kDa Protein-RNA Complex. Angew. Chem. Int. Ed. 52, 9996–10001. https://doi.org/10.1002/anie.201304779.

Marchanka, A., Simon, B., Althoff-Ospelt, G., Carlomagno, T., 2015. RNA structure determination by solid-state NMR spectroscopy. Nat. Commun. 6 https://doi.org/10.1038/ncomms8024.

Marchanka, A., Kreutz, C., Carlomagno, T., 2018a. Isotope labeling for studying RNA by solid-state NMR spectroscopy. J. Biomol. NMR 71, 151–164. https://doi.org/10.1007/s10858-018-0180-7.

Marchanka, A., Stanek, J., Pintacuda, G., Carlomagno, T., 2018b. Rapid access to RNA resonances by proton-detected solid-state NMR at >100 kHz MAS. Chem. Commun. 54, 8972–8975. https://doi.org/10.1039/c8cc04437f.

Martin-Tumasz, S., Reiter, N.J., Brow, D.A., Butcher, S.E., 2010. Structure and functional implications of a complex containing a segment of U6 RNA bound by a domain of Prp24. RNA 16, 792–804. https://doi.org/10.1261/rna.1913310.

Mas, G., Crublet, E., Hamelin, O., Gans, P., Boisbouvier, J., 2013. Specific labeling and assignment strategies of valine methyl groups for NMR studies of high molecular weight proteins. J. Biomol. NMR 57, 251–262. https://doi.org/10.1007/s10858-013-9785-z.

Mas, G., Guan, J.Y., Crublet, E., Debled, E.C., Moriscot, C., Gans, P., Schoehn, G., Macek, P., Schanda, P., Boisbouvier, J., 2018. Structural investigation of a chaperonin in action reveals how nucleotide binding regulates the functional cycle. Sci. Adv. 4, 1–10. https://doi.org/10.1126/sciadv.aau4196.

McDermott, A.E., Polenova, T., Böckmann, A., Zilm, K.W., Paulsen, E.M., Martin, R.W., Montelione, G.T., 2000. Partial NMR assignments for uniformly (13 C, 15 N)-enriched BPTI in the solid state. J. Biomol. NMR 16, 209–219. https://doi.org/10.1023/A.

Mehta, A.K., Shayo, Y., Vankayalapati, H., Hurley, L.H., Schaefer, J., 2004. Structure of a quinobenzoxazine-G-quadruplex complex by REDOR NMR. Biochemistry 43, 11953–11958. https://doi.org/10.1021/bi049697h.

Merritt, M.E., Sigurdsson, S.T., Drobny, G.P., 1999. Long-range distance measurements to the phosphodiester backbone of solid nucleic acids using 31P–19F REDOR NMR. J. Am. Chem. Soc. 121, 6070–6071. https://doi.org/10.1021/ja984173o.

Miao, Q., Nitsche, C., Orton, H., Overhand, M., Otting, G., Ubbink, M., 2021. Paramagnetic Chemical Probes for Studying Biological Macromolecules. Chem. Rev. https://doi.org/10.1021/acs.chemrev.1c00708.

Milligan, J.F., Uhlenbeck, O.C., 1989. Determination of RNA–Protein Contacts Using Thiophosphate Substitutions. Biochemistry 28, 2849–2855. https://doi.org/10.1021/bi00433a016.

Morag, O., Abramov, G., Goldbourt, A., 2014. Complete chemical shift assignment of the ssDNA in the filamentous bacteriophage fd reports on its conformation and on its interface with the capsid shell. J. Am. Chem. Soc. 136, 2292–2301. https://doi.org/10.1021/ja412178n.

Morag, O., Sgourakis, N.G., Baker, D., Goldbourt, A., 2015. The NMR-Rosetta capsid model of M13 bacteriophage reveals a quadrupled hydrophobic packing epitope. Proc. Natl. Acad. Sci. U. S. A. 112, 971–976. https://doi.org/10.1073/pnas.1415393112.

Nadaud, P.S., Helmus, J.J., Höfer, N., Jaroniec, C.P., 2007. Long-range structural restraints in spin-labeled proteins probed by solid-state nuclear magnetic resonance spectroscopy. J. Am. Chem. Soc. 129, 7502–7503. https://doi.org/10.1021/ja072349t.

Nelissen, F.H.T., van Gammeren, A.J., Tessari, M., Girard, F.C., Heus, H.A., Wijmenga, S. S., 2008. Multiple segmental and selective isotope labeling of large RNA for NMR structural studies. Nucleic Acids Res. 36 https://doi.org/10.1093/nar/gkn397.

Nelissen, F.H.T., Tessari, M., Wijmenga, S.S., Heus, H.A., 2016. Stable isotope labeling methods for DNA. Prog. Nucl. Magn. Reson. Spectrosc. 96, 89–108. https://doi.org/10.1016/j.pnmrs.2016.06.001.

Ngo, T.T.M., Yoo, J., Dai, Q., Zhang, Q., He, C., Aksimentiev, A., Ha, T., 2016. Effects of cytosine modifications on DNA flexibility and nucleosome mechanical stability. Nat. Commun. 7, 1–9. https://doi.org/10.1038/ncomms10813.

Nguyen, T.H.D., Galej, W.P., Bai, X.C., Oubridge, C., Newman, A.J., Scheres, S.H.W., Nagai, K., 2016. Cryo-EM structure of the yeast U4/U6.U5 tri-snRNP at 3.7 Å resolution. Nature 530, 298–302. https://doi.org/10.1038/nature16940.

Olsen, G.L., Louie, E.A., Drobny, G.P., Sigurdsson, S.T., 2003. Determination of DNA minor groove width in distamycin-DNA complexes by solid-state NMR. Nucleic Acids Res. 31, 5084–5089. https://doi.org/10.1093/nar/gkg720.

Olsen, G.L., Edwards, T.E., Deka, P., Varani, G., Sigurdsson, S.T., Drobny, G.P., 2005. Monitoring tat peptide binding to TAR RNA by solid-state 31P–19F REDOR NMR. Nucleic Acids Res. 33, 3447–3454. https://doi.org/10.1093/nar/gki626.

Olsen, G.L., Echodu, D.C., Shajani, Z., Bardaro, M.F., Varani, G., Drobny, G.P., 2008. Solid-state deuterium NMR studies reveal μs-ns motions in the HIV-1 transactivation response RNA recognition site. J. Am. Chem. Soc. 130, 2896–2897. https://doi.org/10.1021/ja0778803.

Olsen, G.L., Bardaro Jr., M.F., Echodu, D.C., Drobny, G.P., Varani, G., 2010. Intermediate Rate Atomic Trajectories of RNA by Solid State NMR Spectroscopy. J. Am. Chem. Soc. 132, 303–308. https://doi.org/10.1021/ja907515s.Intermediate.

Otting, G., 2010. Protein NMR using paramagnetic ions. Annu. Rev. Biophys. 39, 387–405. https://doi.org/10.1146/annurev.biophys.093008.131321.

Park, S.H., Das, B.B., Casagrande, F., Tian, Y., Nothnagel, H.J., Chu, M., Kiefer, H., Maier, K., De Angelis, A.A., Marassi, F.M., Opella, S.J., 2012. Structure of the chemokine receptor CXCR1 in phospholipid bilayers. Nature 491, 779–783. https://doi.org/10.1038/nature11580.

Pell, A.J., Pintacuda, G., Grey, C.P., 2019. Paramagnetic NMR in solution and the solid state. Prog. Nucl. Magn. Reson. Spectrosc. 111, 1–271. https://doi.org/10.1016/j.pnmrs.2018.05.001.

Penzel, S., Oss, A., Org, M.L., Samoson, A., Böckmann, A., Ernst, M., Meier, B.H., 2019. Spinning faster: protein NMR at MAS frequencies up to 126 kHz. J. Biomol. NMR 73, 19–29. https://doi.org/10.1007/s10858-018-0219-9.

Pintacuda, G., Giraud, N., Pierattelli, R., Böckmann, A., Bertini, I., Emsley, L., 2007. Solid-state NMR spectroscopy of a paramagnetic protein: Assignment and study of human dimeric oxidized CuII-ZnII superoxide dismutase (SOD). Angew. Chem. Int. Ed. 46, 1079–1082. https://doi.org/10.1002/anie.200603093.

Riedel, K., Leppert, J., Ohlenschläger, O., Görlach, M., Ramachandran, R., 2005a. Characterisation of hydrogen bonding networks in RNAs via magic angle spinning solid state NMR spectroscopy. J. Biomol. NMR 31, 331–336. https://doi.org/10.1007/s10858-005-1614-6.

Riedel, K., Leppert, J., Ohlenschläger, O., Görlach, M., Ramachandran, R., 2005b. TEDOR with adiabatic inversion pulses: Resonance assignments of 13C/15N labelled RNAs. J. Biomol. NMR 31, 49–57. https://doi.org/10.1007/s10858-004-6066-x.

Riedel, K., Herbst, C., Häfner, S., Leppert, J., Ohlenschläger, O., Swanson, M.S., Görlach, M., Ramachandran, R., 2006. Constraints on the structure of (CUG)97 RNA from magic-angle-spinning solid-state NMR spectroscopy. Angew. Chem. Int. Ed. 45, 5620–5623. https://doi.org/10.1002/anie.200600769.

Rosenzweig, R., Kay, L.E., 2014. Bringing dynamic molecular machines into focus by methyl-TROSY NMR. Annu. Rev. Biochem. 83, 291–315. https://doi.org/10.1146/annurev-biochem-060713-035829.

Roy, S., Caruthers, M., 2013. Synthesis of DNA/RNA and their analogs via phosphoramidite and H-phosphonate chemistries. Molecules 18, 14268–14284. https://doi.org/10.3390/molecules181114268.

Schledorn, M., Malär, A.A., Torosyan, A., Penzel, S., Klose, D., Oss, A., Org, M.L., Wang, S., Lecoq, L., Cadalbert, R., Samoson, A., Böckmann, A., Meier, B.H., 2020. Protein NMR Spectroscopy at 150 kHz Magic-Angle Spinning Continues To Improve Resolution and Mass Sensitivity. ChemBioChem 21, 2540–2548. https://doi.org/10.1002/cbic.202000341.

Schlundt, A., Tants, J.N., Sattler, M., 2017. Integrated structural biology to unravel molecular mechanisms of protein-RNA recognition. Methods 118–119, 119–136. https://doi.org/10.1016/j.ymeth.2017.03.015.

Schnitzer, W., Von Ahsen, U., 1997. Identification of specific Rp-phosphate oxygens in the tRNA anticodon loop required for ribosomal P-site binding. Proc. Natl. Acad. Sci. U. S. A. 94, 12823–12828. https://doi.org/10.1073/pnas.94.24.12823.

Schubeis, T., Le, T., Andreas, L.B., Pintacuda, G., 2018. 1H magic-angle spinning NMR evolves as a powerful new tool for membrane proteins. J. Magn. Reson. 287, 140–152. https://doi.org/10.1016/j.jmr.2017.11.014.

Scott, L.G., Geierstanger, B.H., Williamson, J.R., Hennig, M., 2004. Enzymatic synthesis and 19F NMR studies of 2-fluoroadenine- substituted RNA. J. Am. Chem. Soc. 126, 11776–11777. https://doi.org/10.1021/ja047556x.

Sergeyev, I.V., Day, L.A., Goldbourt, A., McDermott, A.E., 2011. Chemical shifts for the unusual DNA structure in Pf1 bacteriophage from dynamic-nuclear-polarization-enhanced solid-state NMR spectroscopy. J. Am. Chem. Soc. 133, 20208–20217. https://doi.org/10.1021/ja2043062.

Shahid, S.A., Markovic, S., Linke, D., Van Rossum, B.J., 2012. Assignment and secondary structure of the YadA membrane protein by solid-state MAS NMR. Sci. Rep. 2, 1–10. https://doi.org/10.1038/srep00803.

Shi, L., Lake, E.M.R., Ahmed, M.A.M., Brown, L.S., Ladizhansky, V., 2009. Solid-state NMR study of proteorhodopsin in the lipid environment: Secondary structure and dynamics. Biochim. Biophys. Acta - Biomembr. 1788, 2563–2574. https://doi.org/10.1016/j.bbamem.2009.09.011.

Siemer, A.B., Huang, K.Y., McDermott, A.E., 2012. Protein Linewidth and Solvent Dynamics in Frozen Solution NMR. PLoS ONE 7. https://doi.org/10.1371/journal.pone.0047242.

Siemer, A.B., McDermott, A.E., 2008. Solid-state NMR on a type III antifreeze protein in the presence of ice. J. Am. Chem. Soc. 130, 17394–17399. https://doi.org/10.1021/ja8047893.

Simon, B., Kirkpatrick, J.P., Eckhardt, S., Reuter, M., Rocha, E.A., Andrade-Navarro, M. A., Sehr, P., Pillai, R.S., Carlomagno, T., 2011. Recognition of 2′-o-methylated 3′-end of piRNA by the PAZ domain of a Piwi protein. Structure 19, 172–180. https://doi.org/10.1016/j.str.2010.11.015.

Smith, J.S., Nikonowicz, E.P., 2000. Phosphorothioate substitution can substantially alter RNA conformation. Biochemistry 39, 5642–5652. https://doi.org/10.1021/bi992712b.

Sodickson, D.K., Levitt, M.H., Vega, S., Griffin, R.G., 1993. Broad band dipolar recoupling in the nuclear magnetic resonance of rotating solids. J. Chem. Phys. 98, 6742–6748. https://doi.org/10.1063/1.464766.

Sprangers, R., Kay, L.E., 2007. Quantitative dynamics and binding studies of the 20S proteasome by NMR. Nature 445, 618–622. https://doi.org/10.1038/nature05512.

Studelska, D.R., Klug, C.A., Beusen, D.D., McDowell, L.M., Schaefer, J., 1996. Long-range distance measurements of protein binding sites by rotational-echo double-resonance NMR. J. Am. Chem. Soc. 118, 5476–5477. https://doi.org/10.1021/ja951509a.

Su, Y., Andreas, L., Griffin, R.G., 2015. Magic angle spinning NMR of proteins: High-frequency dynamic nuclear polarization and 1H detection. Annu. Rev. Biochem. 84, 465–497. https://doi.org/10.1146/annurev-biochem-060614-034206.

Szeverenyi, N.M., Sullivan, M.J., Maciel, G.E., 1982. Observation of spin exchange by two-dimensional fourier transform 13C cross polarization-magic-angle spinning. J. Magn. Reson. 47, 462–475. https://doi.org/10.1016/0022-2364(82)90213-X.

Takegoshi, K., Nakamura, S., Terao, T., 1999. 13C–13C polarization transfer by resonant interference recoupling under magic-angle spinning in solid-state NMR. Chem. Phys. Lett. 307, 295–302. https://doi.org/10.1016/s0009-2614(99)00533-3.

Takegoshi, K., Nakamura, S., Terao, T., 2001. 13C–1H dipolar-assisted rotational resonance in magic-angle spinning NMR. Chem. Phys. Lett. 344, 631–637. https://doi.org/10.1021/ja016789a.

Tamaki, H., Egawa, A., Kido, K., Kameda, T., Kamiya, M., Kikukawa, T., Aizawa, T., Fujiwara, T., Demura, M., 2016. Structure determination of uniformly 13C, 15N labeled protein using qualitative distance restraints from MAS solid-state 13C-NMR observed paramagnetic relaxation enhancement. J. Biomol. NMR 64, 87–101. https://doi.org/10.1007/s10858-015-0010-0.

Tugarinov, V., Hwang, P.M., Ollerenshaw, J.E., Kay, L.E., 2003. Cross-correlated relaxation enhanced 1H–13C NMR spectroscopy of methyl groups in very high

molecular weight proteins and protein complexes. J. Am. Chem. Soc. 125, 10420–10428. https://doi.org/10.1021/ja030153x.
Tycko, R., 2011. Solid-state NMR studies of amyloid fibril structure. Annu. Rev. Phys. Chem. 62, 279–299. https://doi.org/10.1146/annurev-physchem-032210-103539.
Tzakos, A.G., Easton, L.E., Lukavsky, P.J., 2007. Preparation of large RNA oligonucleotides with complementary isotope-labeled segments for NMR structural studies. Nat. Protoc. 2, 2139–2147. https://doi.org/10.1038/nprot.2007.306.
Van Melckebeke, H., Wasmer, C., Lange, A., Ab, E., Loquet, A., Böckmann, A., Meier, B. H., 2010. Atomic-resolution three-dimensional structure of HET-s(218–289) amyloid fibrils by solid-state nmr spectroscopy. J. Am. Chem. Soc. 132, 13765–13775. https://doi.org/10.1021/ja104213j.
Wagner, G., Pardi, A., Wüthrich, K., 1983. Hydrogen Bond Length in 1H NMR Chemical Shifts in Proteins. J. Am. Chem. Soc. 105, 5948–5949. https://doi.org/10.1021/ja00356a056.
Wang, A.C., Kennedy, M.A., Reid, B.R., Drobny, G.P., 1994. A Solid-State 2H NMR Investigation of Purine Motion in a 12 Base Pair RNA Duplex. J. Magn. Reson. B 105, 1–10. https://doi.org/10.1006/jmrb.1994.1092.
Wiegand, T., Cadalbert, R., Gardiennet, C., Timmins, J., Terradot, L., Böckmann, A., Meier, B.H., 2016. Monitoring ssDNA Binding to the DnaB Helicase from Helicobacter pylori by Solid-State NMR Spectroscopy. Angew. Chem. Int. Ed. 55, 14164–14168. https://doi.org/10.1002/anie.201607295.
Wiegand, T., Lacabanne, D., Keller, K., Cadalbert, R., Lecoq, L., Yulikov, M., Terradot, L., Jeschke, G., Meier, B.H., Böckmann, A., 2017a. Solid-state NMR and EPR Spectroscopy of Mn2+-Substituted ATP-Fueled Protein Engines. Angew. Chem. Int. Ed. 56, 3369–3373. https://doi.org/10.1002/anie.201610551.
Wiegand, T., Liao, W.C., Ong, T.C., Däpp, A., Cadalbert, R., Copéret, C., Böckmann, A., Meier, B.H., 2017b. Protein–nucleotide contacts in motor proteins detected by DNP-enhanced solid-state NMR. J. Biomol. NMR 69, 157–164. https://doi.org/10.1007/s10858-017-0144-3.
Wiegand, T., Cadalbert, R., Lacabanne, D., Timmins, J., Terradot, L., Böckmann, A., Meier, B.H., 2019. The conformational changes coupling ATP hydrolysis and translocation in a bacterial DnaB helicase. Nat. Commun. 10, 1–11. https://doi.org/10.1038/s41467-018-07968-3.
Wiegand, T., Lacabanne, D., Torosyan, A., Boudet, J., Cadalbert, R., Allain, F.H.T., Meier, B.H., Böckmann, A., 2020a. Sedimentation Yields Long-Term Stable Protein Samples as Shown by Solid-State NMR. Front. Mol. Biosci. 7, 1–8. https://doi.org/10.3389/fmolb.2020.00017.
Wiegand, T., Schledorn, M., Malär, A.A., Cadalbert, R., Däpp, A., Terradot, L., Meier, B. H., Böckmann, A., 2020b. Nucleotide Binding Modes in a Motor Protein Revealed by 31P- and 1H-Detected MAS Solid-State NMR Spectroscopy. ChemBioChem 21, 324–330. https://doi.org/10.1002/cbic.201900439.
Wilhelm, M., Feng, H., Tracht, U., Spiess, H.W., 1998. 2D CP/MAS 13C Isotropic Chemical Shift Correlation Established by 1H Spin Diffusion. J. Magn. Reson. 134, 255–260. https://doi.org/10.1006/jmre.1998.1512.
Williams, D.J., Boots, J.L., Hall, K.B., 2001. Thermodynamics of 2′-ribose substitutions in UUCG tetraloops. RNA 7, 44–53. https://doi.org/10.1017/S1355838201001558.
Williamson, M.P., 2013. Using chemical shift perturbation to characterise ligand binding. Prog. Nucl. Magn. Reson. Spectrosc. 73, 1–16. https://doi.org/10.1016/j.pnmrs.2013.02.001.
Xue, S., Wang, R., Yang, F., Terns, R.M., Terns, M.P., Zhang, X., Maxwell, E.S., Li, H., 2010. Structural basis for substrate placement by an archaeal box C/D ribonucleoprotein particle. Mol. Cell 39, 939–949. https://doi.org/10.1016/j.molcel.2010.08.022.
Yadav, D.K., Lukavsky, P.J., 2016. NMR solution structure determination of large RNA-protein complexes. Prog. Nucl. Magn. Reson. Spectrosc. 97, 57–81. https://doi.org/10.1016/j.pnmrs.2016.10.001.
Yang, Y., Xiang, S., Liu, X., Pei, X., Wu, P., Gong, Q., Li, N., Baldus, M., Wang, S., 2017. Proton-detected solid-state NMR detects the inter-nucleotide correlations and architecture of dimeric RNA in microcrystals. Chem. Commun. 53, 12886–12889. https://doi.org/10.1039/c7cc07483b.
Yip, K.M., Fischer, N., Paknia, E., Chari, A., Stark, H., 2020. Atomic-resolution protein structure determination by cryo-EM. Nature 587, 157–161. https://doi.org/10.1038/s41586-020-2833-4.
Yu, L.J., McDowell, L.M., Poliks, B., Studelska, D.R., Cao, C., Potter, G.S., Schaefer, J., Song, F., Stivers, J.T., 2004. Recognition of an unnatural difluorophenyl nucleotide by uracil DNA glycosylase. Biochemistry 43, 15429–15438. https://doi.org/10.1021/bi0483864.
Yu, T.Y., Schaefer, J., 2008. REDOR NMR Characterization of DNA Packaging in Bacteriophage T4. J. Mol. Biol. 382, 1031–1042. https://doi.org/10.1016/j.jmb.2008.07.077.
Zehnder, J., Cadalbert, R., Terradot, L., Ernst, M., Böckmann, A., Güntert, P., Meier, B.H., Wiegand, T., 2021. Paramagnetic Solid-State NMR to Localize the Metal-Ion Cofactor in an Oligomeric DnaB Helicase. Chem. - A Eur. J. 27, 7745–7755. https://doi.org/10.1002/chem.202100462.
Zhao, X., 2012. Protein Structure Determination by Solid-State NMR. Top. Curr. Chem. 326, 187–213. https://doi.org/10.1007/128_2011_287.
Zhao, S., Yang, Y., Zhao, Y., Li, X., Xue, Y., Wang, S., 2019. High-resolution solid-state NMR spectroscopy of hydrated non-crystallized RNA. Chem. Commun. 55, 13991–13994. https://doi.org/10.1039/c9cc06552k.
Zhou, D.H., Rienstra, C.M., 2008. High-performance solvent suppression for proton detected solid-state NMR. J. Magn. Reson. 192, 167–172. https://doi.org/10.1016/j.jmr.2008.01.012.
Zhou, D.H., Shah, G., Cormos, M., Mullen, C., Sandoz, D., Rienstra, C.M., 2007a. Proton-detected solid-state NMR spectroscopy of fully protonated proteins at 40 kHz magic-angle spinning. J. Am. Chem. Soc. 129, 11791–11801. https://doi.org/10.1021/ja073462m.
Zhou, D.H., Shea, J.J., Nieuwkoop, A.J., Franks, W.T., Wylie, B.J., Mullen, C., Sandoz, D., Rienstra, C.M., 2007b. Solid-state protein-structure determination with proton-detected triple-resonance 3D magic-angle-spinning NMR spectroscopy. Angew. Chem. Int. Ed. 46, 8380–8383. https://doi.org/10.1002/anie.200702905.
Zwahlen, C., Legault, P., Vincent, S.J.F., Greenblatt, J., Konrat, R., Kay, L.E., 1997. Methods for measurement of intermolecular NOEs by multinuclear NMR spectroscopy: Application to a bacteriophage λ N-peptide/boxB RNA complex. J. Am. Chem. Soc. 119, 6711–6721. https://doi.org/10.1021/ja970224q.